

See discussions, stats, and author profiles for this publication at: <https://www.researchgate.net/publication/347302562>


The role and significance of juvenile sediments in the formation of A-type granites, West Junggar oceanic arc (NW China): zircon Hf-O isotopic perspectives


Article in *Geological Society of America Bulletin* · December 2020


CITATIONS


0

12 authors, including:

 **Jiyuan Yin**
Chinese Academy of Geological Sciences
31 PUBLICATIONS 576 CITATIONS
[SEE PROFILE](#)


 **Wenjiao Xiao**
Chinese Academy of Sciences
629 PUBLICATIONS 25,433 CITATIONS
[SEE PROFILE](#)

 **Min Sun**
The University of Hong Kong
313 PUBLICATIONS 26,172 CITATIONS
[SEE PROFILE](#)

 **Wen Chen**
Chinese Academy of Geological Sciences
114 PUBLICATIONS 1,862 CITATIONS
[SEE PROFILE](#)

Some of the authors of this publication are also working on these related projects:

 □□□□□□□□-□□□□□□□□□□□□□□□□□ [View project](#)

 Geological and Geophysical Survey in the Iranian Plateau [View project](#)

The role and significance of juvenile sediments in the formation of A-type granites, West Junggar oceanic arc (NW China): Zircon Hf-O isotopic perspectives

Jiyuan Yin^{1,2,†}, Wenjiao Xiao^{3,4}, Christopher J. Spencer⁵, Min Sun², Wen Chen¹, Huiqing Huang⁶, Chao Yuan⁷, Yunying Zhang², He Huang¹, Xiaoping Xia⁷, and Zaili Tao¹

¹Key Laboratory of Deep-Earth Dynamics of Ministry of Natural Resources, Institute of Geology, Chinese Academy of Geological Sciences, Beijing 100037, China

²Department of Earth Sciences, University of Hong Kong, Pokfulam Road, Hong Kong, China

³Xinjiang Research Center for Mineral Resources, Xinjiang Institute of Ecology and Geography, Chinese Academy of Sciences, Urumqi 830011, China

⁴State Key Laboratory of Lithospheric Evolution, Institute of Geology and Geophysics, Chinese Academy of Sciences, Beijing 100029, China

⁵Department of Geological Sciences and Geological Engineering, Queen's University, Kingston, Ontario K7L 3N6, Canada

⁶Economic Geology Research Centre, College of Science and Engineering, James Cook University, Townsville QLD 4814, Australia

⁷State Key Laboratory of Isotope Geochemistry, Guangzhou Institute of Geochemistry, Chinese Academy of Sciences, Guangzhou 510640, China

ABSTRACT

Oceanic arc subduction systems are the loci of substantial recycling of oceanic crust and production of juvenile arc crust that differentiates to more evolved felsic crust. Inevitably, some juvenile sediments are subducted with the oceanic crust. However, distinguishing the incorporation of juvenile sediments in oceanic arcs is not always straightforward, because they may not measurably shift many geochemical signatures, such as Sr and Nd isotopes, of oceanic arcs. Nevertheless, combined zircon U-Pb, Hf, and O isotope data can provide a powerful tool to decipher sedimentary flux into oceanic arc magmas, and here we report a case study for the late Paleozoic A-type granites from the West Junggar oceanic arc in the southern Central Asian Orogenic Belt. These plutons contain hastingsite and iron biotite diagnostic minerals and have high alkali, FeO_T/MgO, Zr, and Ga/Al, but possess low CaO contents, and strongly negative Eu, Sr, and Ba anomalies, demonstrating their close affinity with A-type granites. Zircon U-Pb analyses indicate that these A-type granites emplaced in the Late Carboniferous to Early Permian (ca. 307–298 Ma). Their high zircon εHf_(t) values (+12.4 to +15.5), suggest that the mag-


mas were derived from a mantle or juvenile crustal source. However, their δ¹⁸O_{Zrn} (+7.2‰ to +11.9‰) values are significantly higher than that of the mantle, and modeling using Hf-O isotope and rare earth element data indicate the assimilation of sedimentary materials at a proportion of ~50%. Our data suggest that juvenile sediments (e.g., greywacke) played an important role in the formation of the studied A-type granites. The re-melting of sedimentary material induced by the late Carboniferous ridge subduction can promote the transition from an intra-oceanic arc to continental crust. Our results show that the subduction and re-melting of juvenile sediments in oceanic arc systems could be an important mechanism for the maturation of oceanic arc crust.

INTRODUCTION

A-type granites were originally defined as being alkaline, anhydrous, and have an anorogenic affinity (Loiselle and Wones, 1979). They are chemically characterized by high total-alkali, Zr, and Ga contents; and have low CaO, Ba, Eu, and Sr contents; and high FeO_T/MgO and Ga/Al values (Whalen et al., 1987). A-type granites are considered to crystallize from relatively high-temperature magmas and occur in both continental and oceanic crust. There have been debates over the genesis of A-type granites for a long time. Different mechanisms have been proposed

to explain the origin of A-type magmas (e.g., melting of an underplated lower crust or recycled oceanic crust or granulitic metasedimentary rocks, fractionation from mantle-derived basaltic magmas, or mixing of crust- and mantle-derived magma) (Eby, 1992; Collins et al., 1982; Whalen et al., 1987; Frost et al., 2002; Bonin, 2007; Huang et al., 2011; Yang et al., 2017). However, within oceanic arc systems, all components including sediments, mafic lower crust, oceanic crust, and mantle-derived basaltic magma have similar radiogenic isotopic signatures (Bindeman et al., 2005; Tatsumi et al., 2008). Large volumes of juvenile crust are created and recycled through subduction processes culminating in the formation of felsic magma (i.e., A-type granite) (e.g., Tatsumi et al., 2008; Tani et al., 2011; Tang et al., 2019). In oceanic arc systems, studies using the conventional radiogenic isotopic methods are unable to distinguish the granitic melts from juvenile sediment, recycled oceanic crust, or mafic lower crust (Lackey et al., 2005; Jeon et al., 2012).

Zircon is a common and highly refractory accessory mineral in felsic lithologies and preserves the isotopic compositions of its parent magmas at the time of crystallization (Valley et al., 1994; Bindeman, 2008). Zircon Hf isotopic compositions can distinguish magma sources made of juvenile crust versus old crustal materials (Kemp et al., 2006; Dhuime et al., 2011), but cannot discern surficial processes that the source may have previously suffered, as the Hf

Jiyuan Yin  <http://orcid.org/0000-0003-3554-7674>
†yinjyuan1983@163.com.

isotopic system is not easily modified by hydrothermal alteration or weathering (Griffin et al., 2000; Harrison et al., 2005). In contrast, oxygen isotopic data are useful in tracing the recycling of supracrustal rocks, because oxygen isotopes (expressed as $\delta^{18}\text{O}$) are fractionated by low-temperature processes (Lackey et al., 2005), and thus the weathering and erosion of juvenile mantle-derived rocks can significantly alter their $\delta^{18}\text{O}$ values, while their Sr-Nd-Hf isotopic compositions are essentially unchanged (McCulloch et al., 1980).

In this contribution, we report combined in situ isotopic analyses on zircon (O, U-Pb, Hf isotopes) from the late Paleozoic A-type granites in the West Junggar oceanic arc, southern Central Asian Orogenic Belt (CAOB). The results provide critical information regarding the magma genesis that cannot be revealed by Hf or O isotopes alone. These A-type granites provide a unique opportunity for detecting the role of recycled juvenile sediments in the formation of A-type granites and constraining the mechanism of crustal maturation in the oceanic arc system.

GEOLOGICAL SETTING AND SAMPLING

The CAOB is the largest accretionary orogenic belt on earth. Voluminous granites and volcanic rocks in the CAOB are characterized by positive $\epsilon\text{Nd}_{(t)}$ and $\epsilon\text{Hf}_{(t)}$ values (Jahn et al., 2000; Tang et al., 2012), and represents a site of major crustal growth in the Phanerozoic (Fig. 1A; Jahn et al., 2000; Xiao et al., 2008; Han et al., 2015; Han and Zhao, 2018). As an important component of the CAOB, the West Junggar oceanic arc is highlighted by great exposures of Paleozoic ophiolitic mélanges and subduction-related arc magmatic rocks. No metamorphic basement has been identified (Xiao et al., 2008), and the dominant Carboniferous volcanic strata are composed of basalts, andesitic basalts, and andesites (Geng et al., 2011). The volcanic rocks display consistently depleted whole-rock Sr-Nd isotopic compositions (i.e., $\epsilon\text{Nd}_{(t)} = +4.2$ to $+7.7$) (Geng et al., 2011). The volcanogenic sediments also show depleted zircon Hf isotopic compositions (i.e., $\epsilon\text{Hf}_{(t)} = +6$ to $+15.7$) (Choulet et al., 2012). The detrital zircon U-Pb geochronology ages from late Paleozoic sedimentary rocks in the West Junggar suggest that volcanogenic sediments were deposited in the Early to Late Carboniferous at 356–304 Ma (Choulet et al., 2012; Liu et al., 2017). Abundant Late Carboniferous to Early Permian granitic plutons intruded Devonian–Carboniferous strata (Geng et al., 2009; Tang et al., 2012), which were in turn intruded by mafic to intermediate dikes (Fig. 1B, Yin et al., 2010, 2013). Previous geochemical and

Sr-Nd-Hf isotopic studies have demonstrated that the Late Carboniferous to Early Permian granites were mantle-derived (Han et al., 1997; Geng et al., 2009; Tang et al., 2012). However, it is unclear whether the sources of these magmas are made of juvenile supracrustal materials, juvenile ocean crust, or mantle-derived basaltic magma. Also, it is widely accepted that these granites reflect crustal growth, but the geodynamic setting of the granite formation and the associated modes for crustal growth are the subjects of an ongoing debate. One view suggested that Late Carboniferous to Early Permian granites were generated in a post-collisional setting (Han et al., 1997; Chen and Arakawa, 2005; Chen et al., 2010). More recent views have also proposed important contribution from late Paleozoic ridge subduction in the region (Geng et al., 2009; Tang et al., 2010, 2012; Yin et al., 2010, 2013, 2015).

Samples from six representative granitic batholiths (i.e., Wuerkashier, Northern Keramay, Tiechanggou, Miaoergou, Hatu, and Akebasitao), located in the southern West Junggar, and were collected for geochemical and isotopic investigation in this study (Fig. 1B). Representative photographs of field outcrops and hand specimens are shown in Figure 2. They intruded the Middle Devonian to Lower Carboniferous strata. These granites are massive and medium- to coarse-grained. They show pink or light-yellow color at outcrops. The northern Keramay granite sample (18NKM01) has the mineral assemblages of perthite (55–60 vol%), albite (~15 vol%), quartz (~25 vol%), biotite (~3–5 vol%), hastingsite (~1 vol%) and the accessory minerals of magnetite, apatite, zircon, titanite, and orthite (Fig. 3A). The granite sample (WJ1144) was collected from the Miaoergou batholith, composed of orthoclase (~70 vol%), albite (~3–5 vol%), quartz (20–25 vol%), hastingsite (3–5 vol%), biotite (1–3 vol%), and minor accessory minerals (e.g., magnetite, apatite, zircon, titanite, and orthite; Fig. 3B). The granite sample (WJ1117) was collected from the southern slope of the Wuerkashier Mountains, consisting of perthite and orthoclase (65–70 vol%), albite (~5 vol%), quartz (20–25 vol%), hastingsite (3–5 vol%), biotite (1–2 vol%), and minor accessory minerals (e.g., magnetite, apatite, zircon, titanite, and orthite; Fig. 3C). Tiechanggou granite sample (18TCG01) consists of perthite (~55 vol%), albite (~15 vol%), quartz (25–30 vol%), hastingsite (~1 vol%), and biotite (3–5 vol%) (Fig. 3D) with accessory minerals of magnetite, apatite, zircon, titanite, and allanite. The granite sample (18Hatu) was collected from the Hatu pluton, composed of perthite (50–55 vol%), albite (~15 vol%), quartz (25–30 vol%), hastingsite (2–3 vol%), biotite (3–5 vol%), and

minor accessory minerals (e.g., magnetite, apatite, zircon, titanite, and orthite; Fig. 3E). The granite sample (18AK01) was collected from the Akebasitao pluton. They consist of perthite (~55 vol%), albite (~15 vol%), quartz (~25 vol%), hastingsite (3–5 vol%), biotite (1–3 vol. vol%), and minor accessory minerals (e.g., magnetite, apatite, zircon, titanite, and orthite; Fig. 3F). Dark-colored enclaves are observed in the above granite samples, ranging from a few centimeters to tens of centimeters and showing sharp contacts with the host granites (Fig. 2F). The sampling locations are shown in Figure 1B and the GPS coordinates, ages, and isotopic compositions of all samples are summarized in Table S1¹.

ANALYTICAL METHODS

LA-ICP-MS Zircon U-Pb Dating

The U-Pb isotopic compositions of zircon grains for samples 18AK01, 18HATU, and 18NKM01 were analyzed on a Nu Instruments multicollector–inductively coupled plasma–mass spectrometer (LA-ICP-MS), attached to a Resonetics RESOLUTION M-50-HR Excimer Laser Ablation System in the Department of Earth Sciences, University of Hong Kong. Most analyses were carried out with a beam diameter of 30 μm , at a 6 Hz repetition rate. This gave a ^{238}U signal of 3×10^4 to 200×10^4 counts per second, depending on U contents. Typical ablation time was 30–60 s, resulting in pits 20 to 40 μm deep. Before measurement, samples were ablated for 10 s to eliminate potential contamination on sample surfaces. Also, ^{202}Hg was monitored to control the isobaric interference of ^{204}Hg on ^{204}Pb . Data acquisition started with a 15 s measurement of a gas blank during the laser warm-up time. The ^{204}Pb signal was so small that the common lead correction is therefore regarded as unnecessary (Xia et al., 2004). The standard zircon 91500 was used to evaluate the magnitude of mass bias and inter-elemental fractionation. The 91500 standard zircon was used as primary

¹Supplemental Material. Table S1: Summary of zircon Lu-Hf-O isotope data from the late Carboniferous to early Permian granitoids in the West Junggar oceanic arc (NW China); Table S2: LA-ICP-MS U-Pb isotopic analysis for zircon grains from the granitic batholiths in the West Junggar oceanic arc (NW China); Table S3: Major and trace element compositions of the granitic batholiths in the West Junggar oceanic arc (NW China); and Table S4: Lu-Hf-O isotopic compositions of zircon grains from the granitic batholiths in the West Junggar oceanic arc (NW China). Please visit <https://doi.org/10.1130/GSAB.S.13244348> to access the supplemental material, and contact editing@geosociety.org with any questions.

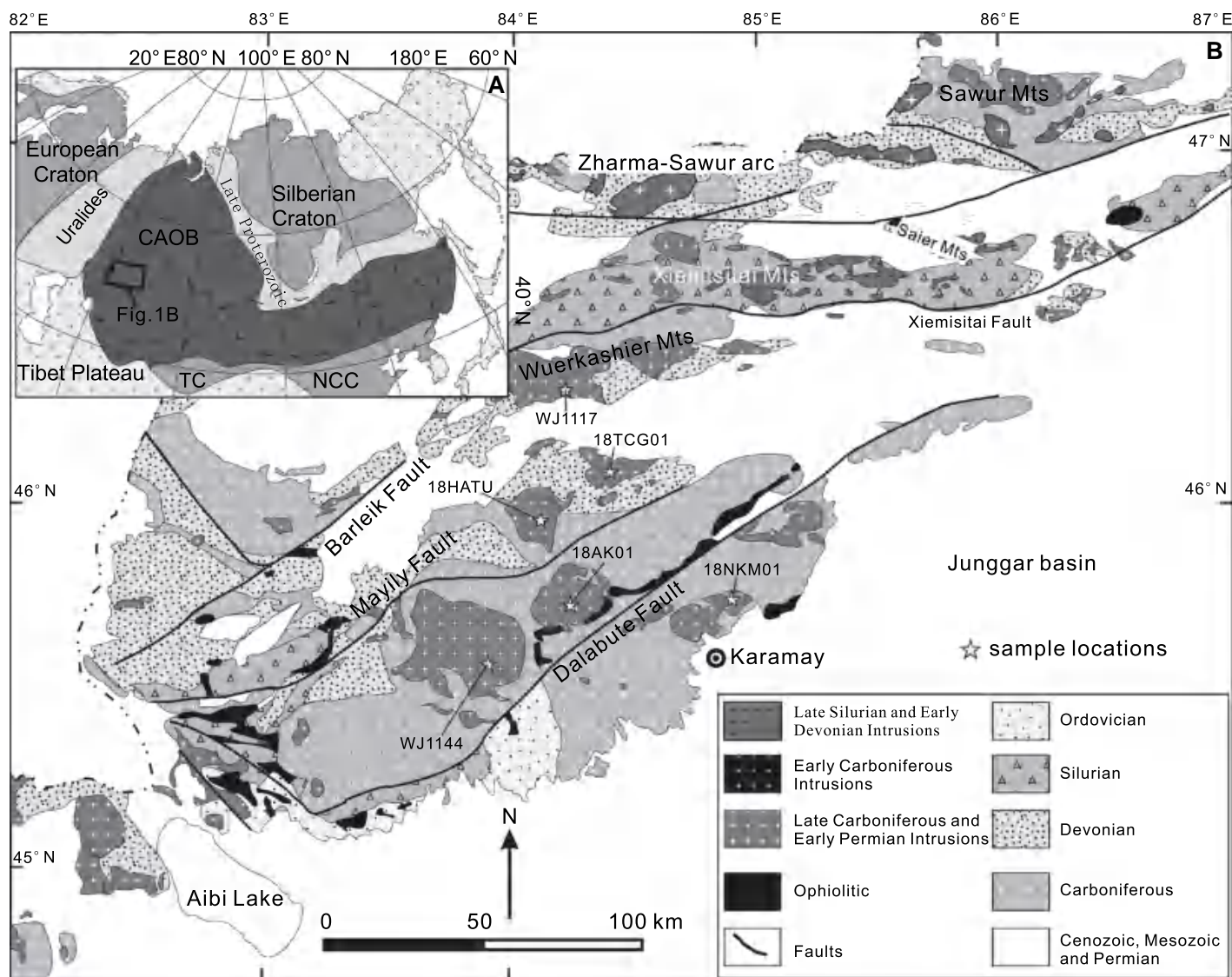


Figure 1. (A) Simplified tectonic divisions of the Central Asian Orogenic Belt (CAOB) (after Jahn et al., 2000). (B) Geological map of the west-ern Junggar region, NW China (modified after Yin et al., 2013, 2017). TC—Tarim Craton; NCC—North China Craton; Mts—Mountains.

reference material for all U-Pb age determinations, while zircon Plešovice was used as an unknown sample. During the analyses in this study, 20 measurements on Plešovice zircon yielded a weighted $^{206}\text{Pb}/^{238}\text{U}$ age of 337.2 ± 6.1 Ma, which is in good agreement with the recommended U-Pb age (337 Ma) (Sláma et al., 2008). The instrumental settings and detailed analytical procedures are described in Xia et al. (2004). The U-Pb ages were calculated using the U decay constants of $^{238}\text{U} = 1.55125 \times 10^{-10} \text{ year}^{-1}$, $^{235}\text{U} = 9.8454 \times 10^{-10} \text{ year}^{-1}$, and the Isoplot 3 software (Ludwig, 2003). Individual analyses are presented with 1σ errors, and uncertainties in pooled age results are quoted at the 95% confidence level (2σ). $^{206}\text{Pb}/^{238}\text{U}$ ages are adopted in this study because the relatively small

amount of ^{207}Pb accumulated in “young” zircons (<1000 Ma) does not permit precise $^{207}\text{Pb}/^{206}\text{Pb}$ determination (Black et al., 2003).

Zircon U-Pb isotopic analysis for samples WJ1144, WJ1117, and 18TCG01 were conducted at Nanjing FocuMS Technology Co. Ltd. Australian Scientific Instruments RESOLUTION LR S-155 laser-ablation system and Agilent Technologies 7700x quadrupole ICP-MS were combined for the experiments. The 193 nm ArF excimer laser, homogenized by a set of beam delivery systems, was focused on the zircon surface with a fluence of 5.0 J/cm^2 . Each acquisition incorporated 20 s background (gas blank), followed by a spot diameter of $33 \mu\text{m}$ at 8 Hz repetition rate for 40 s (equating to 320 pulses). Helium was applied as the carrier

gas to efficiently transport aerosol out of the ablation cell and was mixed with argon via T-connector before entering the ICP torch. Dwell times were set to 20 ms for ^{207}Pb , 15 ms for ^{206}Pb and ^{208}Pb , and 10 ms for ^{232}Th and ^{238}U . Ablation occurred in intervals of eight sample zircons, directly preceded and followed by two zircon 91500 as external standards and one zircon GJ-1 as quality control. During the analyses in this study, 10 measurements on zircon GJ-1 yielded a weighted $^{206}\text{Pb}/^{238}\text{U}$ age of 603 ± 4 Ma (1σ), which is in good agreement with the recommended U-Pb age (599.8 ± 4.5 Ma, Jackson et al., 2004). ICPMSDataCal software 8.0 (Liu et al., 2010) was used to select off-line raw data, integrate background and analytical signals, time-drift correct, and quantitatively calibrate

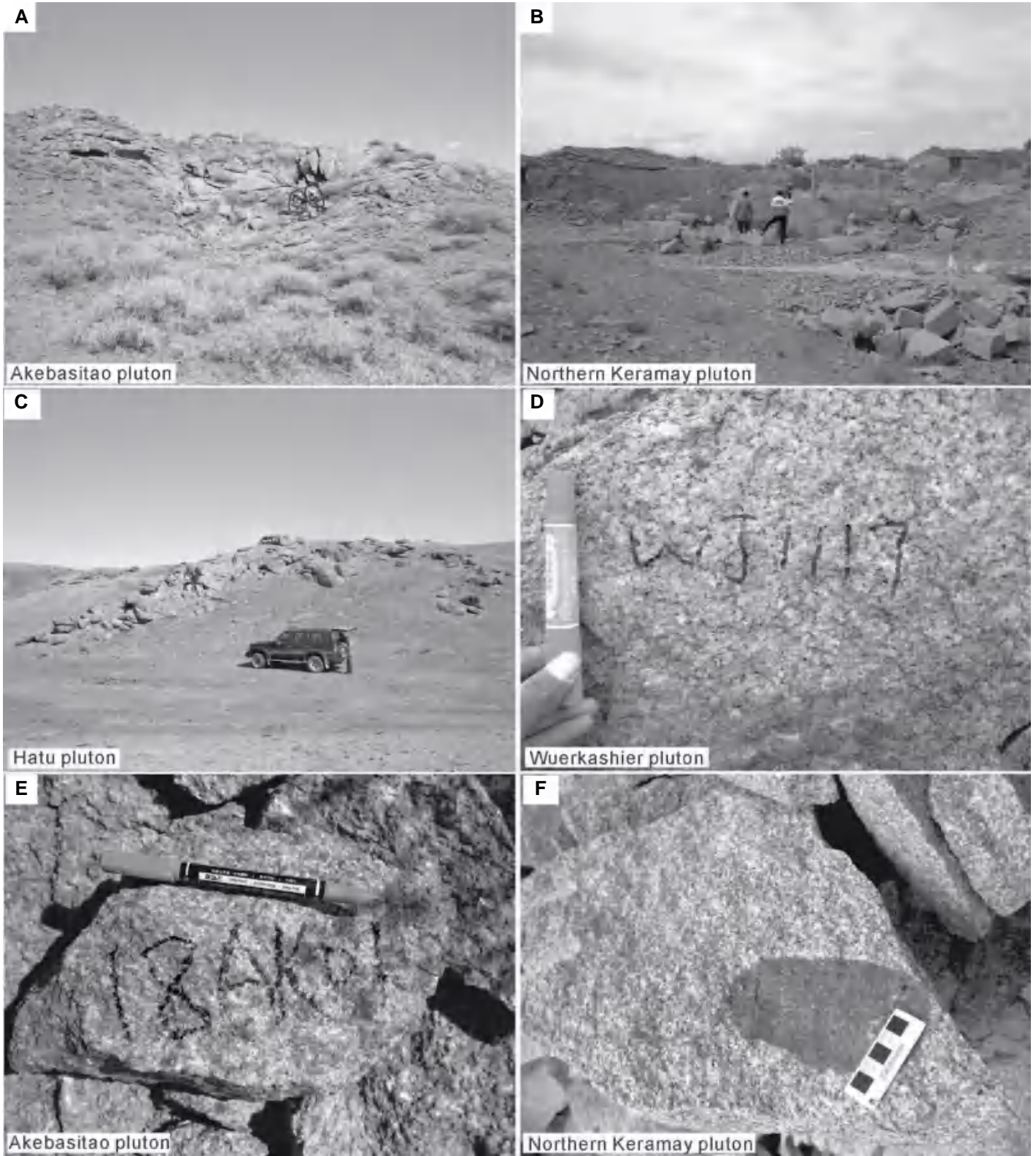


Figure 2. Field photos of rocks from the representative granitic batholiths in West Junggar, NW China. (A, E) Outcrop and hand specimen of Akebasitao alkaline granite; (B) Outcrop of the northern Keramay alkaline granite; (C) Outcrop of Hatu alkaline granite; (D) Hand specimen of Wuerkashier alkaline granite; (F) Dark colored enclave in the northern Keramay alkaline granite.

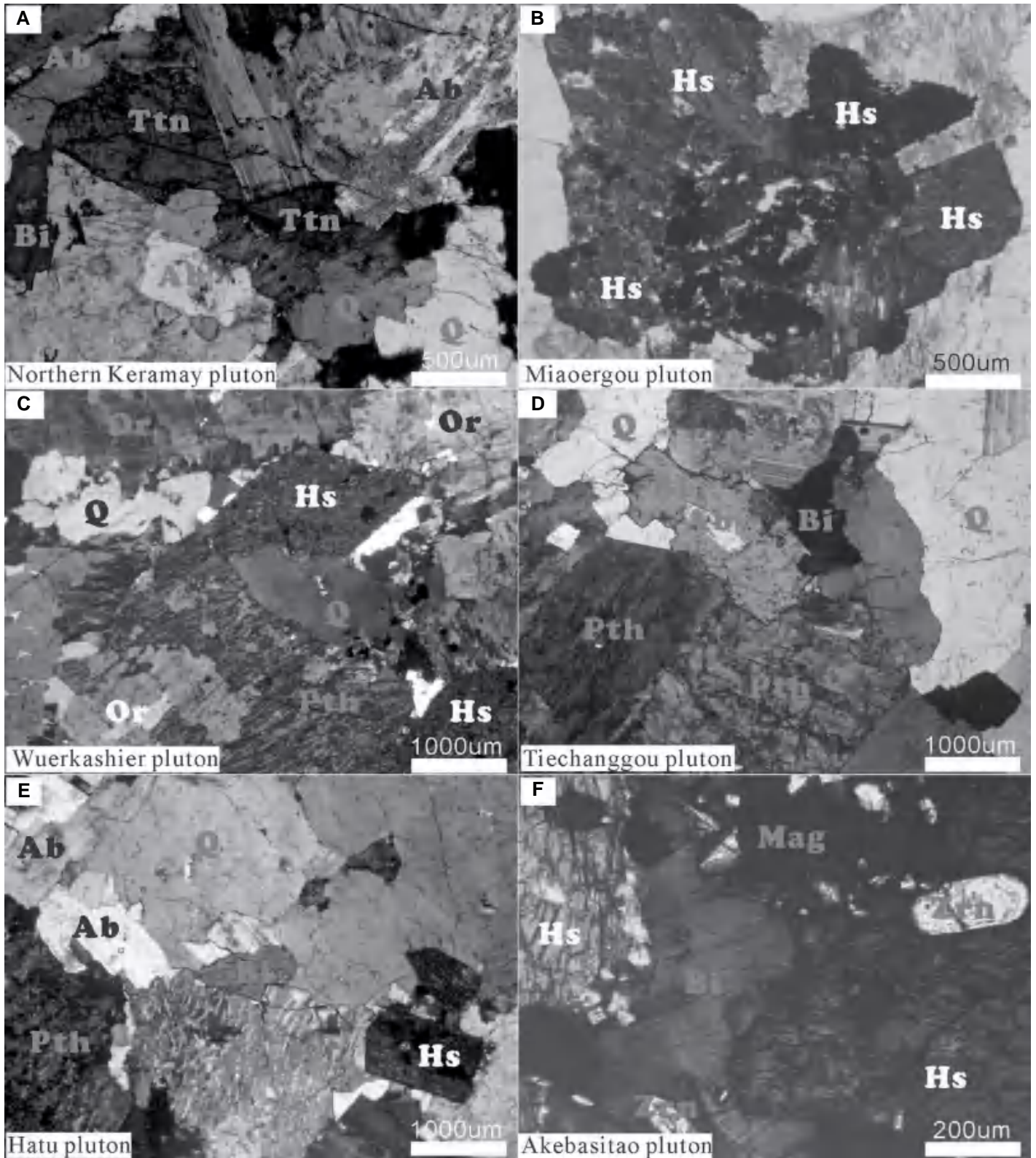


Figure 3. Microscopic photos of rocks from the granitic batholiths in the West Junggar, NW China. Mag—Magnetite; HS—Hastingsite; Zrn—Zircon; Ab—Albite; Or—Orthoclase; Pth—Perthite; Tnt—Titanite; Bi—Biotite; and Q—Quartz.

U-Pb isotopes. Common lead correction was conducted following the method of Andersen (2002). Concordia diagram plotting, probability density plotting, and weighted average age calculation were accomplished using Isoplot 3.27 (Ludwig, 2003).

LA-MC-ICP-MS Zircon Lu-Hf Isotope Analysis

Zircon Lu-Hf isotopic ratio analyses were conducted following U-Pb analyses on the relatively big zircon grains with concordant U-Pb ages for placing two laser ablation pits. Lu-Hf analysis spots were undertaken on the same cathodoluminescence (CL) domain and as closely as possible to the U-Pb analysis spots. Australian Scientific Instruments RESOLUTION LR S-155 laser-ablation system and Nu Plasma II MC-ICP-MS were combined for the experiments at Nanjing FocuMS Co. Ltd. Ablation protocol employed 20 s background (gas blank) and a spot diameter of 50 μm at 8 Hz repetition rate for 40 s (equating to 320 pulses). Zircon GJ-1 was used as the reference standard and gave a weighted average $^{176}\text{Hf}/^{177}\text{Hf}$ ratio of 0.282008 ± 0.000004 (2σ , $n = 35$), indistinguishable from the ratio of 0.282000 ± 0.000005 (2σ) by solution analysis method (Morel et al., 2008). ϵHf values were calculated based on the present-day chondritic $^{176}\text{Hf}/^{177}\text{Hf}$ ratio of 0.282772 and $^{176}\text{Lu}/^{177}\text{Hf}$ ratio of 0.0332 (Blichert-Toft and Albarede, 1997).

SIMS Zircon O Isotope Analysis

Zircon oxygen isotopes were measured using the Cameca IMS-1280 HR secondary ion mass spectrometer (SIMS) at State Key Laboratory of Isotope Geochemistry, Guangzhou Institute of Geochemistry, Chinese Academy of Sciences, Guangzhou, China. The detailed analytical procedures were similar to those described by Yang et al. (2018). The $^{133}\text{Cs}^+$ primary ion beam with an intensity of ~ 2 nA was accelerated at 10 kV and focused to an area of 10 μm on the sample surface and the size of analytical spots is ~ 20 μm in diameter (10 μm beam diameter + 10 μm raster). Oxygen isotopes were measured in multicollector mode using two off-axis Faraday cups. Total analytical time per spot was ~ 3.5 min, including 30 s of pre-sputtering, 120 s of automatic tuning of the secondary beam, and 64 s of analysis. The measured oxygen isotopic data were corrected for instrumental mass fractionation using the Penglai zircon standard ($\delta^{18}\text{O}$ Vienna standard mean ocean water = 5.3‰; Li et al., 2010b), which was analyzed once every four unknowns, using the sample-standard bracketing method. The internal precision of a single analysis generally was better than 0.1‰

(1σ) for the $^{18}\text{O}/^{16}\text{O}$ ratio. As discussed by Kita et al. (2009), internal precision for a single spot (commonly $<0.1\%$, 1σ) is not a good index of analytical quality for stable isotope ratios measured by SIMS. Therefore, the external precision, measured by the spot-to-spot reproducibility of repeated analyses of the Penglai standard, 0.35‰ (2 standard deviations (SD), $n = 30$) is adopted for data evaluation. Thirty measurements of the Qinghu zircon standard during the course of this study yielded a weighted mean of $\delta^{18}\text{O} = 5.45 \pm 0.11\%$ (2SD), which is consistent within errors with the reported value of $5.4 \pm 0.2\%$ (Li et al., 2013).

Whole-Rock Geochemistry Analysis

Bulk-rock major elements were measured by X-ray fluorescence spectrometry (XRF), and trace elements were measured by inductively coupled plasma-mass spectrometry (ICP-MS) and inductively coupled plasma-atomic emission spectrometry (ICP-AES) at the ALS Chemex Co., Ltd., Guangzhou. Samples were fused with lithium metaborate-lithium tetraborate flux, which also included an oxidizing agent (lithium nitrate), and then the samples were poured into a platinum mold. The resultant disk was then analyzed by XRF spectrometry. The analytical accuracy and precision of the XRF analyses are $<5\%$ for major elements. XRF analysis was performed in conjunction with a loss on ignition analysis at 1000 °C. For XRF, a prepared sample was added to the lithium metaborate/lithium tetraborate flux, mixed well, and fused

in a furnace at 1025 °C. Then, the resulting melt was cooled and dissolved in an acid mixture containing nitric, hydrochloric, and hydrofluoric acids. This solution was then analyzed by ICP-MS. A prepared sample was digested with perchloric, nitric, hydrofluoric, and hydrochloric acids. The residue was topped up with dilute hydrochloric acid, and the resulting solution was analyzed by ICP-AES. The results were corrected for spectral interelement interferences.

RESULTS

Zircon U-Pb Geochronology

The zircon U-Pb isotopic data are given in Table S2 (see footnote 1). Most zircon grains are 80–200 μm in length with length/width ratios of 1:1–2:1 and display oscillatory zoning in CL images (Fig. 4). The analyzed zircon grains from all samples show variable U (60–3080 ppm) and Th (17–758 ppm) contents with Th/U ratios ranging from 0.19 to 0.96, indicating a magmatic origin. The U-Pb data is summarized in Figure 5. The 22, 26, 27, 19, and 27 analytical spots of zircon grains from the granite samples WJ1117, WJ1144, 18AK01, 18HATU, 18NKM01, and 18TCG01 yielded weighted mean $^{206}\text{Pb}/^{238}\text{U}$ ages of 298.3 ± 1.8 Ma ($n = 22$, mean square weighted deviation [MSWD] = 0.9), 302.3 ± 1.9 Ma ($n = 26$, MSWD = 0.9), 305.4 ± 1.3 Ma ($n = 27$, MSWD = 0.1), 301.8 ± 1.4 Ma ($n = 19$, MSWD = 0.1), 304.5 ± 1.4 Ma ($n = 27$, MSWD = 0.1), and 306.6 ± 1.8 Ma ($n = 22$, MSWD = 0.8), respectively (Figs. 5A–5F). All

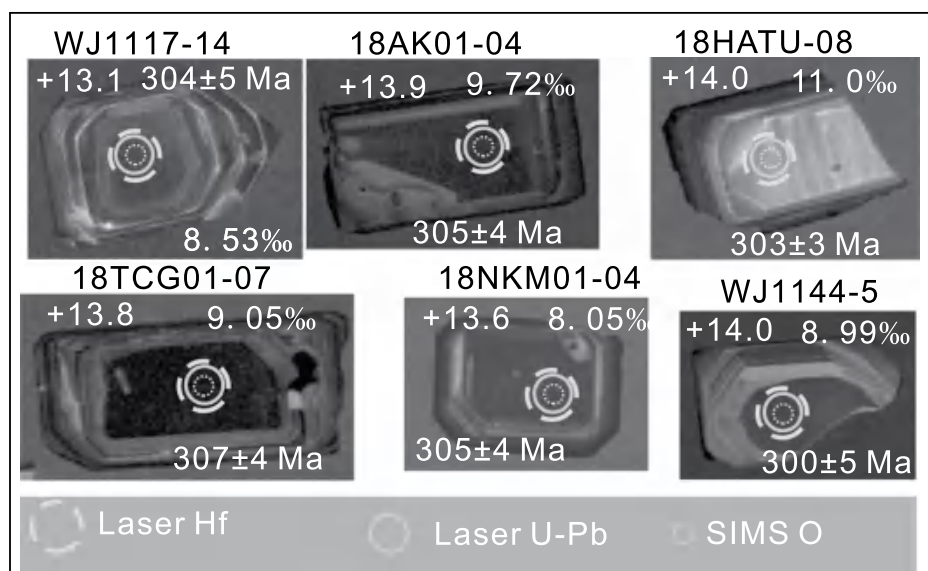


Figure 4. Cathodoluminescence images of representative zircon grains analyzed for U-Pb and O isotopes of the granites in the West Junggar, NW China. SIMS—secondary ion mass spectrometry.

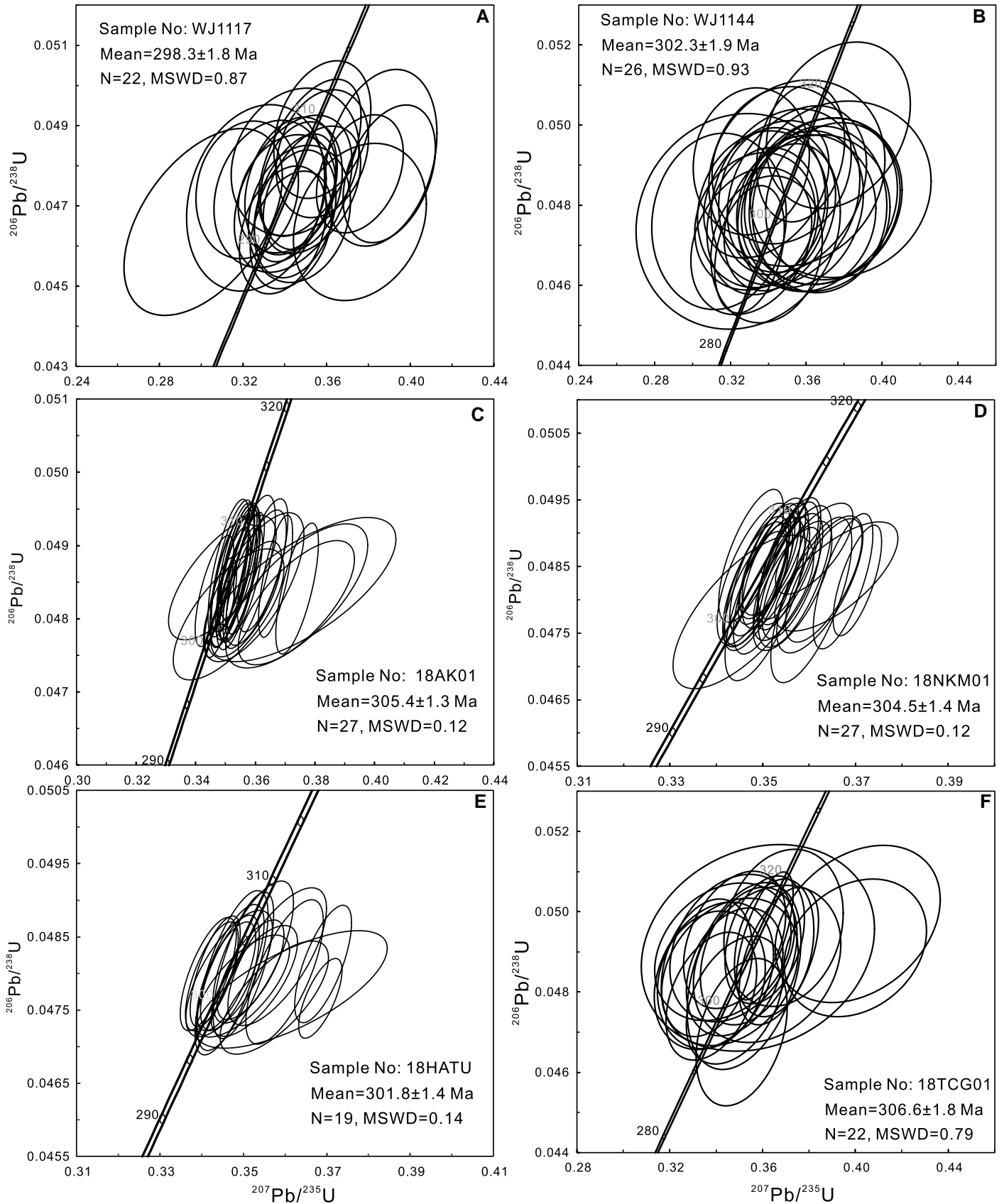


Figure 5. U-Pb concordia diagrams showing zircon ages obtained by laser ablation–inductively coupled plasma–mass spectrometry for the granites in the West Junggar, NW China.

weighted means correspond to single populations without any data over dispersion (Spencer et al., 2016).

Major and Trace Element Geochemistry

Whole-rock major and trace element compositions are given in Table S3 (see footnote 1). All samples of the granitic intrusions from the West Junggar show similar geochemical characteristics. They have high SiO₂ (71.4–78.4 wt%), total alkali (Na₂O + K₂O = 7.9–9.6 wt%) contents and low Al₂O₃ (10.7–14.5 wt%), MgO (0.01–0.5 wt%), FeO_T (0.9–2.5 wt%), CaO (0.4–1.7 wt%), and P₂O₅ (0.02–0.08 wt%)

contents, and plot in the field of high-K calc-alkaline series (Fig. 6A). Accordingly, they have high FeO_T/(FeO_T + MgO) (0.8–1.0) and (K₂O + Na₂O)/CaO (5–21) values, mainly falling in the ferroan field (Fig. 6B). In the total alkali versus silica diagram, all samples are sub-alkaline and plot in the granite field (Fig. 6D). They show low A/CNK (0.91–1.04) values (A/CNK = molecular Al₂O₃/(CaO + Na₂O + K₂O)), indicating metaluminous to weakly peraluminous compositions (Fig. 6D). These granites have high total rare earth element (REE) contents and show relatively flat normalized REE patterns (La/Yb)_N = 2.7–8.1) with pronounced negative Eu anomalies

(Eu/Eu* (Eu_N/√(Sm_N × Gd_N)) = 0.1–0.5) (Fig. 7A). They have high concentrations of high field strength elements (e.g., Zr, Th, and U) and large-ion lithophile elements (e.g., K, Rb, and Ba) and show negative Nb, Ta, Sr, P, and Ti anomalies (Fig. 7B).

Zircon Hf-O Isotopic Geochemistry

The zircon Lu-Hf and O isotopic data for the studied granites are given in Table S4 (see footnote 1). Hf-O isotopic compositions were determined from the same zircon grains with zircon U-Pb analysis. Initial ¹⁷⁶Hf/¹⁷⁷Hf ratios denoted as εHf(t) values, and Hf model

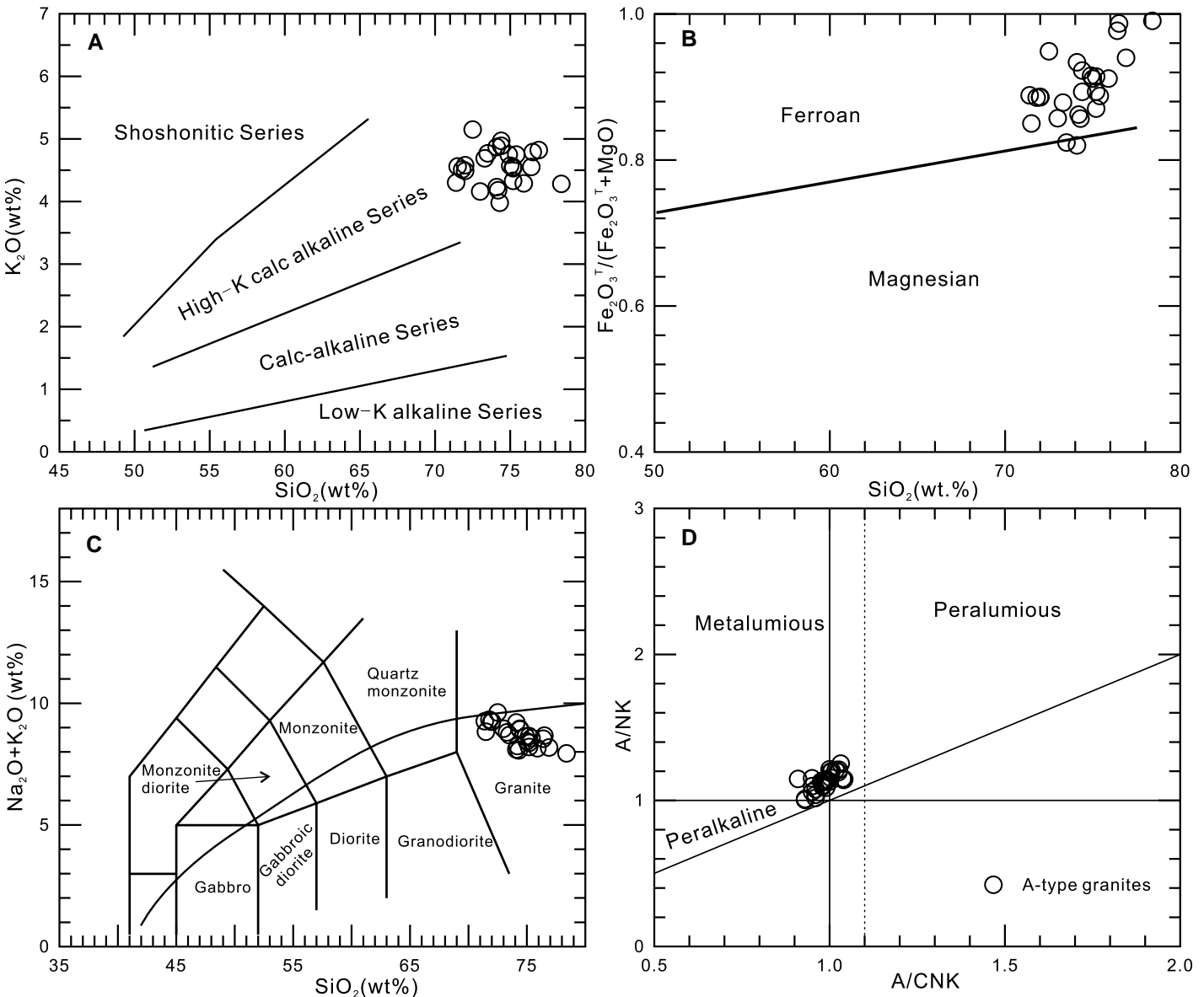


Figure 6. (A) K₂O-SiO₂ classification diagram is after Gill (1981); (B) SiO₂ versus FeO^T/(FeO^T+MgO) (Frost et al., 2001); (C) SiO₂-(Na₂O + K₂O) diagram (Middlemost, 1994); (D) A/NK versus A/CNK (Maniar and Piccoli, 1989), Al/(Ca + Na+K) = Al₂O₃/(CaO + Na₂O + K₂O), Al/(Na+K) = Al₂O₃/(Na₂O + K₂O), molecular ratio.

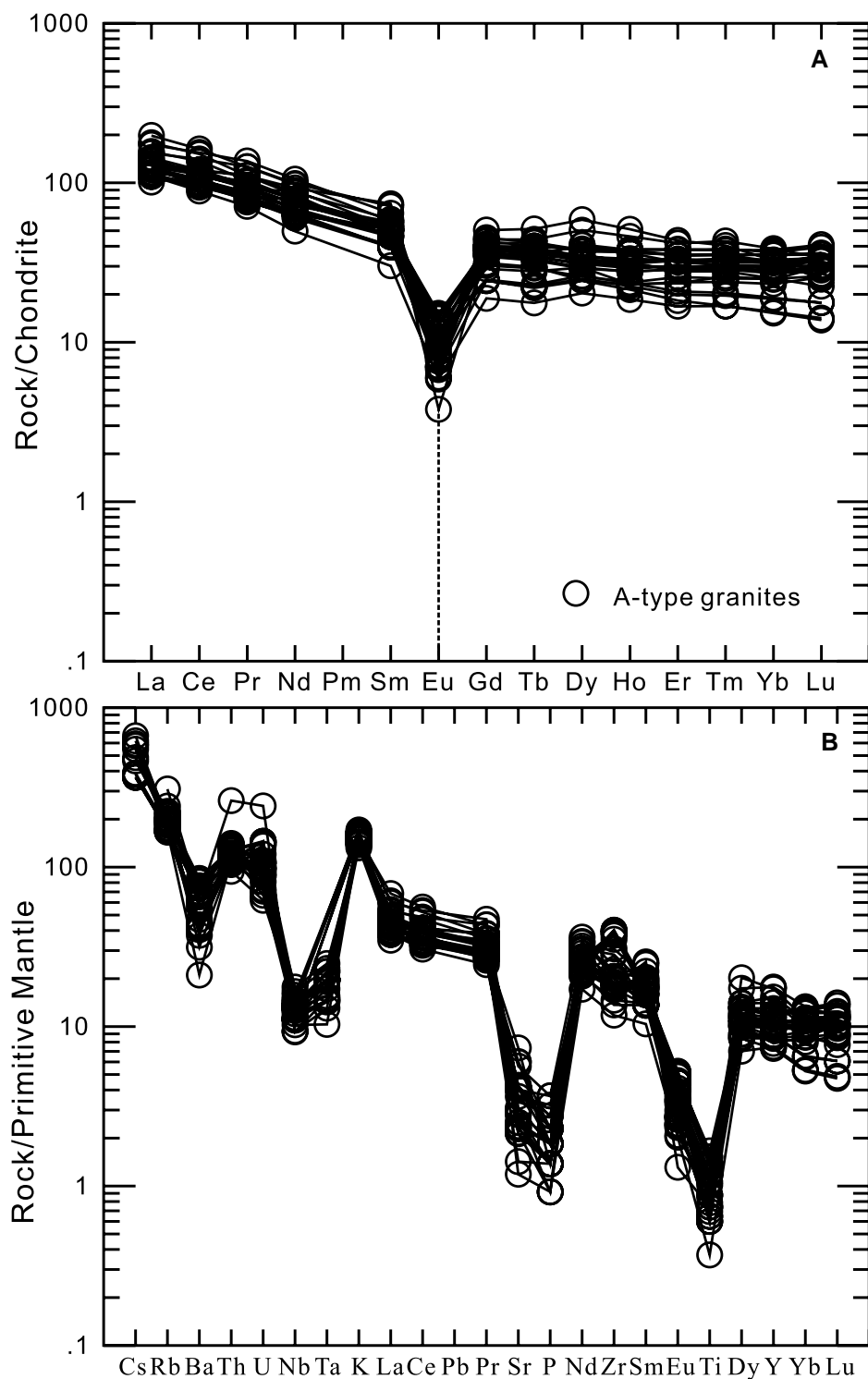


Figure 7. (A) Chondrite-normalized rare earth element patterns. (B) Primitive mantle normalized trace element diagrams for the granitic batholiths in West Junggar, NW China. The chondrite, primitive mantle data are from Sun and McDonough (1989).

ages were also calculated based on crystallization ages from the U-Pb dating (Table S2). All granites are characterized by high $\epsilon\text{Hf}(t_0)$ values (+12.4 to +15.5) and distinctly

young Hf model ages of 328–527 Ma. Zircon oxygen isotopic ratios for these granites are higher in $\delta^{18}\text{O}$ values (7.2‰–11.9‰) than those ($5.3 \pm 0.6\text{‰}$, 2SD) of igneous zircons

occurring in mantle-derived magmas (Valley, 2003).

DISCUSSION

Geochemical Affinities

Granites are generally divided into S-type, I-type, and A-type (Collins et al., 1982; Whalen et al., 1987). Firstly, these granites in the West Junggar differ from strongly peraluminous S-type granites by low A/CNK (<1.1) and absence of muscovite, tourmaline, or garnet (Fig. 6D; Chappell and White, 1992; Barbarin, 1999). Secondly, they display prominent negative Ba, Sr, P, Eu, and Ti anomalies (Figs. 7A and 7B), which, together with their high $10,000 \times \text{Ga/Al}$ ratios and high Zr contents and zircon saturation temperatures ($T_{\text{Zr}} = 794\text{--}906\text{ }^\circ\text{C}$), are distinct from highly fractionated granites and I-type granites, but similar to typical A-type granites (Whalen et al., 1987; Eby, 1990, 1992). Finally, they contain diagnostic minerals (i.e., hastingsite and iron biotite), which also indicate their close affinity with A-type granites (Eby, 1992; Tang et al., 2012; and this study). In the discrimination diagrams of FeO_7/MgO and Zr versus $10,000 \text{ Ga/Al}$, they plot in the A-type granite field of Whalen et al. (1987) (Figs. 8A and 8B). In the Nb-Ce-Y and Nb-Ce-3*Ga diagram, they can be further classified as A_2 -type granites (Eby, 1992) (Figs. 8C and 8D). Therefore, we conclude that the granitic intrusions in this study belong to A_2 -type granites.

Petrogenesis of the A-Type Granites

Petrogenetic models of A-type granite mostly involve differentiation of basaltic magma or partial melting of mafic lower crust (Bonin, 2007; Frost and Frost, 2011). Magmas of this kind of origin will have $\delta^{18}\text{O}_{\text{zm}}$ values equal to or slightly higher than that of mantle zircon ($5.3 \pm 0.6\text{‰}$, 2SD) (e.g., Kemp et al., 2007; Valley, 2003). Partial melting of old crustal components will generate high $\delta^{18}\text{O}_{\text{zm}}$ values (>8.0‰) A-type granites, but with crustal Sr-Nd-Hf isotopic compositions (Huang et al., 2011). The studied A-type granites are metaluminous to weakly peraluminous with aluminum saturation index lower than 1.1 (Fig. 6D; White and Chappell, 1977), and have low initial $^{87}\text{Sr}/^{86}\text{Sr}$ ratios of 0.7030–0.7045, high $\epsilon\text{Nd}(t_0)$ values of +6.3 to +8.5 (Geng et al., 2009; Tang et al., 2012) and high $\epsilon\text{Hf}(t_0)$ values of +12.4 to +15.5 (Table S4). The above isotopic compositions indicate a depleted mantle-like source (Fig. 9A). However, they are characterized by high SiO_2 (71.4–78.4 wt%) and low MgO (0.01–0.45 wt%), Cr (<19 ppm), and Ni

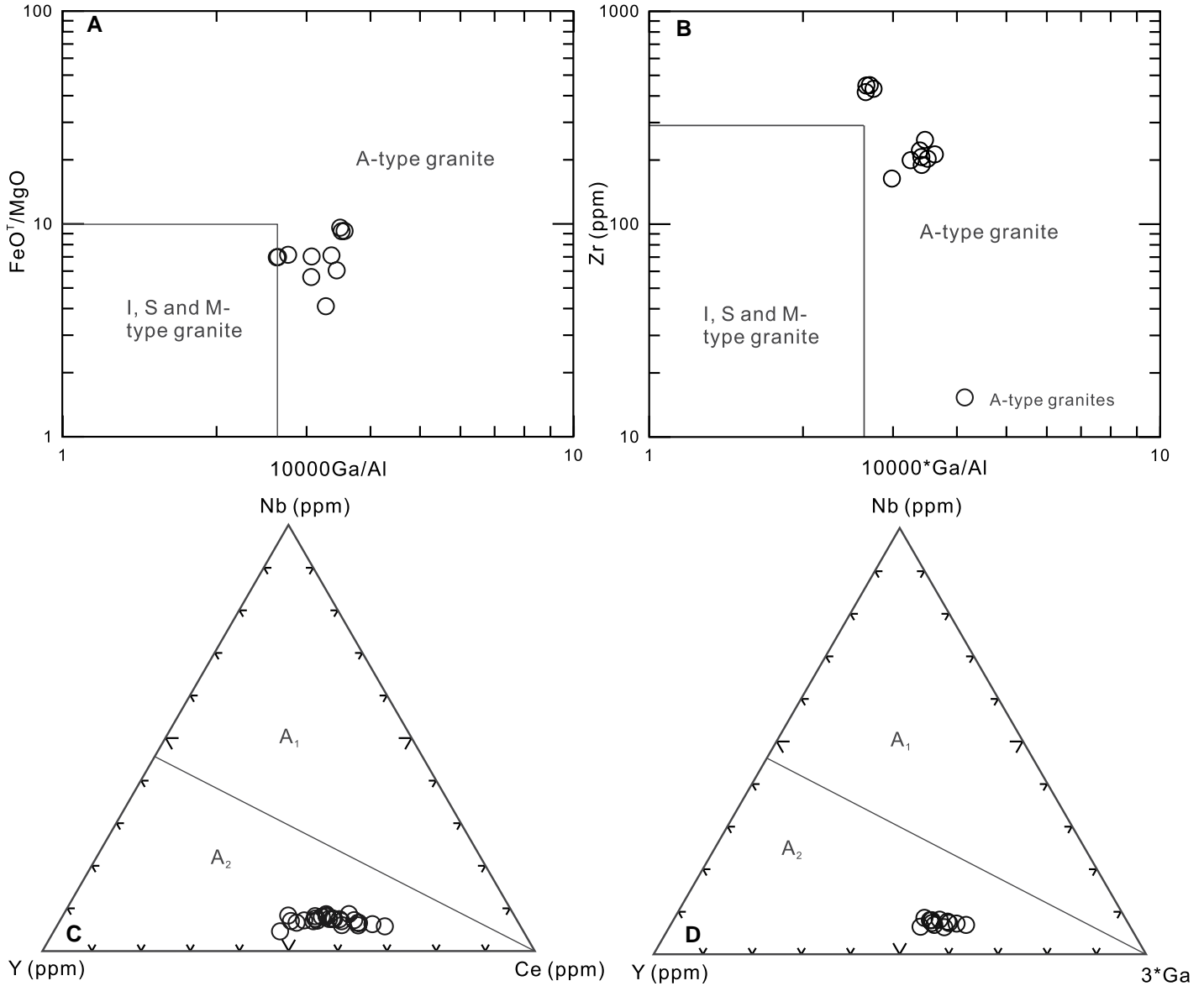


Figure 8. (A and B) FeO^T/MgO and Nb versus 10,000 Ga/Al discrimination diagram (Whalen et al., 1987). (C and D) Discrimination diagrams for the subdivision of the A-type granites by Eby (1992).

(<6 ppm) contents, ruling out the involvement of mantle rocks in the magma source or intensive melt-mantle interaction. A small number of inherited zircon grains have been found in the A-type granites in the West Junggar and their inherited cores yielded mean ages of 329–322 Ma (Geng et al., 2009; Tang et al., 2019), which are similar to those of the Early Carboniferous volcanic rocks or those of detrital zircon from the Early to Late Carboniferous sedimentary rocks (Geng et al., 2011; Choulet et al., 2012). In addition, the Early Carboniferous volcanic rocks consistently display depleted mantle-like Sr-Nd isotopic compositions (initial $^{87}Sr/^{86}Sr$ ratios = 0.7034–0.7054, $\epsilon Nd(t) = +4.2$ to +7.7) (Geng et al., 2011). The Early to Late Carbon-

iferous arc-related volcanogenic sedimentary rocks are composed of greywacke, sandstone, and microconglomerate, all of which have positive zircon $\epsilon Hf(t)$ values of +5 to +17 (85% of the data are between +10 and +16), indicating a depleted mantle-like magma source (Choulet et al., 2012). Thus, the above isotopic data indicate that the studied A-type granites could be derived from the Early Carboniferous to Late Carboniferous arc volcanic/sedimentary rock or the underplated juvenile materials. Zircon is extremely retentive of the magmatic O isotope and zircon in equilibrium with pristine mantle-derived melts have mantle-like $\delta^{18}O_{zrn}$ values ($5.3 \pm 0.6\text{‰}$, 2SD; Valley, 2003). Thus, zircon $\delta^{18}O$ reflects the primary $\delta^{18}O$ of the

magma in which the zircon crystallized, but is much less susceptible to alteration than the O isotopic composition of whole-rock ($\delta^{18}O_{WR}$) (Jeon et al., 2012). In general, the $\delta^{18}O$ values of arc magmas are overlapping or a little bit higher than those of pristine mantle-derived melts ($5.3 \pm 0.6\text{‰}$, 2SD) (Bolhar et al., 2008). The A-type granites in this study have much higher zircon $\delta^{18}O$ values (7.2‰–11.9‰), suggesting the existence of supracrustal rocks in their magma sources (Figs. 9A and 9B; Kemp et al., 2007). Consequently, the zircon Hf and O isotopic data together suggest that juvenile supracrustal material was an important component in the magma source for the studied A-type granites.

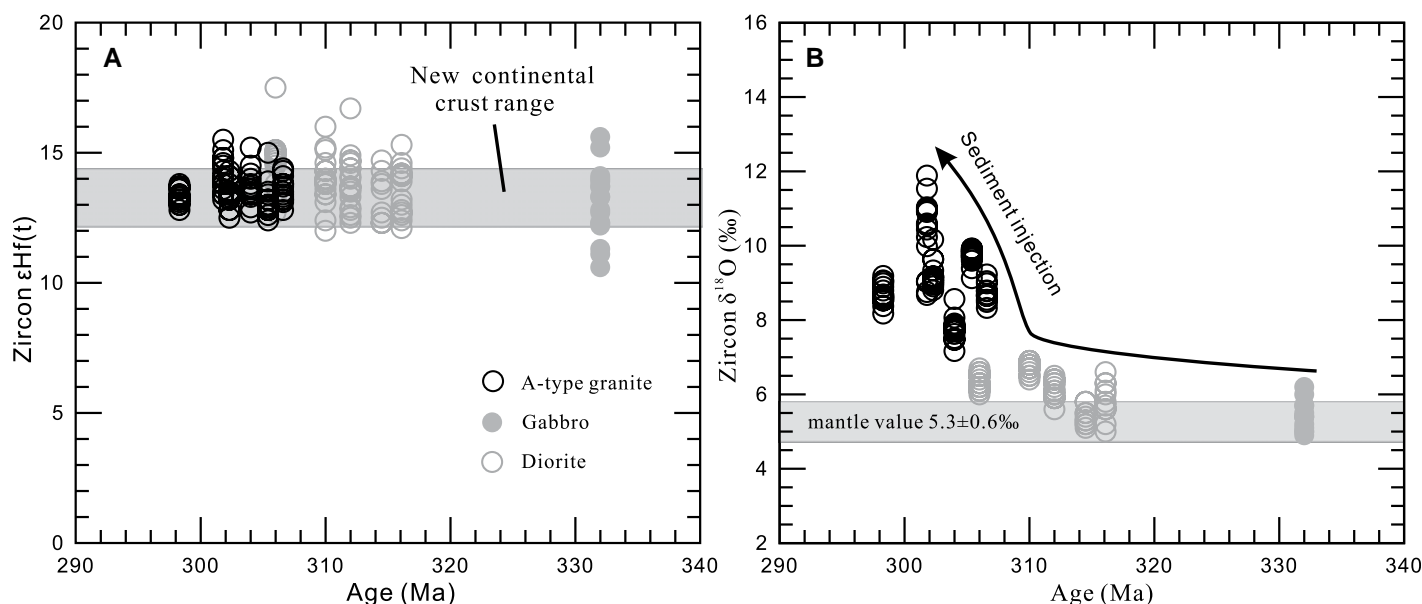


Figure 9. Correlation plots between age and Hf-O isotopic data for the granites in the West Junggar, NW China; $\epsilon Hf_{(t)} = +13.2 \pm 1.1$ is used as the new continental crust ranges (Dhuime et al., 2011). The field of mantle-derived zircon (Valley et al., 2005) is shown for comparison. Hf-O isotopic data of West Junggar gabbro and diorite is from Tang et al. (2019).

Contribution of Juvenile Sediment in the Formation of A-Type Granites

The Paleozoic oceanic subduction-accretion system generated the Early to Late Carboniferous volcanic or sedimentary rocks in the West Junggar. In contrast to magmatic activity at mid-ocean ridges or within-plate settings, arc magmas are highly explosive because of the enrichment of volatile phases. Therefore, the extrusive products of arc volcanism often occur as pyroclastic deposits into intra-arc and arc flanking basins of the adjoining forearc and back-arc (Cawood et al., 2009). Compositional differences of magmas produced by partial melting of different source rocks, such as metabasalts, metatonalites, metagreywackes, and metapelites, under variable melting conditions may be visualized in terms of molar oxide ratios, such as $Al_2O_3/(MgO + FeO_T)$ and $CaO/(MgO + FeO_T)$ (Altherr et al., 2000). The studied A-type granites plot in the source field of metagraywacke (Fig. 10), implying that the magma source of the high $\delta^{18}O_{zrn}$ and high $\epsilon Hf_{(t)}$ A-type granites possibly contained the Early to Late Carboniferous (meta) graywackes. However, previous geochemical studies suggest that most granites, even those considered as typical examples of “S-type” cannot be derived solely from metamorphosed crustal sediments (Collins, 1996; Healy et al., 2004), although the eastern Himalayan leucogranites could be derived solely from crustal sediments (Hopkinson et al., 2017) and they

show typical geochemical characteristics of S-type granites rather than A-type granites. In this study, we used the Junggar Carboniferous metagraywackes as the source to model their melting process, and the results show that the A-type granitic melt cannot be formed by batch melting in any proportion. Given that plagioclase is strongly enriched in Sr and Eu, and garnet is strongly depleted in light-REEs and enriched in heavy-REEs (HREEs) and Y, the distinct negative Sr and Eu anomalies, low La/Yb and Sr/Y ratios of the studied A-type granites likely reflect the presence of residual plagioclase (Pl) with little or without garnet (Grt) in their sources (Fig. 11A). In addition, pressure-temperature conditions

for partial melting of crustal rocks based on experimental data are summarized in the literature (Wang et al., 2016). They indicate that the lower limit of Grt stability is 0.5 GPa, and Pl will disappear at pressures >1.2–1.5 GPa (Rapp et al., 2003; Wang et al., 2016), the studied A-type granites were likely generated by high temperature melting (up to 906 °C) of crustal source rocks in the pressure range of ≤ 0.5 GPa (corresponding to depths of <15 km; Wang et al., 2016). Besides, the West Junggar A-type granites are characterized by relatively high HREE (such as $Yb = 2.6\text{--}6.6$ ppm) and Y ($Y = 24.6\text{--}80.4$ ppm) contents, and negative Eu, Sr, and Ba anomalies, further suggesting that partial melting most likely occurred in a

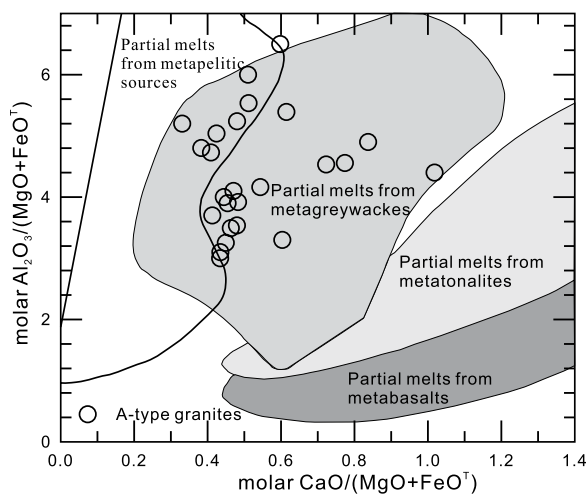


Figure 10. Molar $Al_2O_3/(MgO + FeO^T)$ versus molar $CaO/(MgO + FeO^T)$ diagram for Late Carboniferous to Early Permian A-type granites in the West Junggar, NW China (after Altherr et al., 2000). Data of whole rock major element compositions are from Table S3 (see footnote 1).

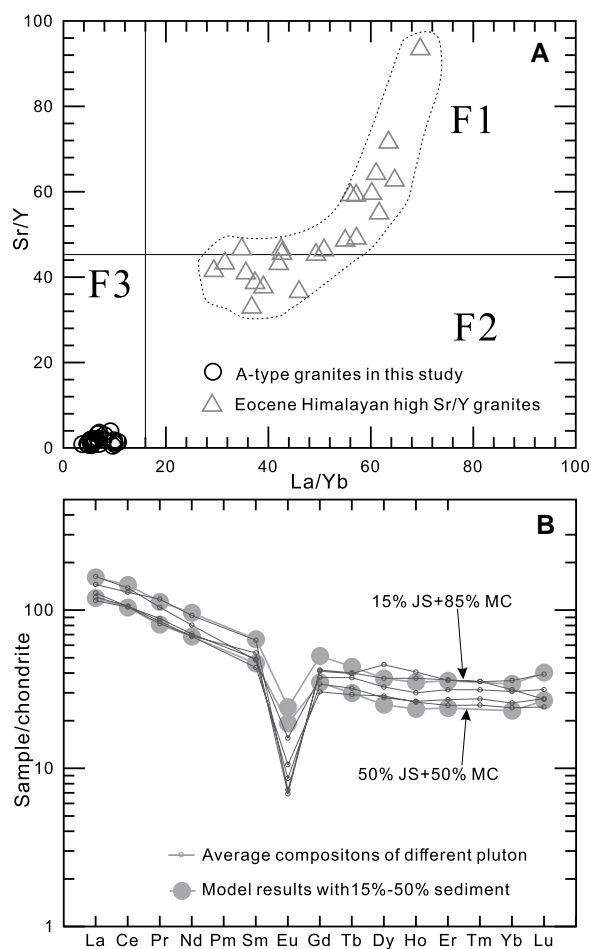


Figure 11. (A) La/Yb versus Sr/Y (Wang et al., 2016). This diagram indicates the effects of residual garnet (Grt) and plagioclase (Pl) during partial melting. F1–F3 are crustal melts in the stability fields of Grt with little or no Pl, with Pl and Grt, and Pl with little or no Grt, respectively. The data of Eocene Himalayan high Sr/Y granites is from Zeng et al. (2011). (B) The trace element composition for different pluton in the West Junggar, NW China. The granites are closely matched by a mixture of 15%–50% greywacke melt and 85%–50% middle crust melt. The trace element compositions of the juvenile sediment (JS) are represented by an average Early Carboniferous greywacke from the northeast Junggar (Tao et al., 2014). The global weighted middle crust component is granodiorite (Rudnick and Gao, 2014). Therefore, the trace element compositions of the middle crust (MC) are represented by the Late Carboniferous granodiorite in the

West Junggar (Chen and Arakawa, 2005). Bulk solid/melt partition coefficients of andesitic-dacitic melts in equilibrium with a Pl residuum (35% clinopyroxene and 65% plagioclase). Individual mineral K_d values are from McKenzie and O’Nions (1991) Bulk solid/melt partition coefficients for sediment melting are from Johnson and Plank (1999). Composition of JS and MC melts are based on the assumption of 20% and 10% batch melting, respectively.

relatively shallow depth (i.e., middle crust) (Figs. 7A and 7B; McKenzie and O’Nions, 1991), and the residual Pl played an important role in their magma genesis. REE modeling assumes that partial melting took place under Pl stability condition without the involvement of Grt and the initial mineralogical assemblages had a clinopyroxene: Pl ratio of 35:65. Our results show that the REE patterns for the West Junggar A-type granites can be successfully reproduced by 10%–20% batch melting with a (15% to 50% sediment plus 85–50% middle crust) melt component (Fig. 11B). Also, a binary mixing calculation for Hf–O isotopes indicates that 15%–50% of juvenile sedimentary rocks were involved in the source of the studied A-type granites (Fig. 12C). Therefore, the proportion of such juvenile sediments may reach ~50% and they can play an important role in the formation of the studied A-type granites.

Implication for Geodynamic Process and Crustal Evolution

The West Junggar accretionary prism was formed during the Early Cambrian to Late Carboniferous with depleted mantle-like Sr–Nd–Hf isotope compositions. Although voluminous granites also outcropped in the West Junggar region, there is no consensus on their origin, and competing petrogenetic models were proposed, including partial melting of a depleted mantle reservoir (Han et al., 1997; Chen and Arakawa, 2005); partial melting of juvenile mafic lower crust (Chen and Jahn, 2004; Geng et al., 2009); and partial melting of residual oceanic crust (Tang et al., 2012). Different models imply different crust formation and evolution processes. Although zircon Hf isotopic compositions of the studied A-type granites are comparable to those of the depleted mantle, their $\delta^{18}\text{O}$ values

of 7.2‰ to +11.9‰ are much higher than those of the mantle, thus juvenile sedimentary rocks must have been involved in the magma source. Therefore, the A-type granites are unlikely generated by partial melting of a depleted mantle reservoir or juvenile lower crust, which will show mantle-like $\delta^{18}\text{O}_{\text{zm}}$ values ($5.3 \pm 0.6\text{‰}$, 2SD; Valley, 2003).

As discussed above, both of REE modeling and binary mixing calculation of Hf–O isotopes indicate that 50% of sedimentary rocks and 50% of middle crust were involved in the source of the studied A-type granites. Obviously, the injection of sediment is very important. The volcanogenic sediments were formed by weathering of volcanic arc and deposited in the adjacent forearc basin or trench (Cawood et al., 2009). The sediments in the trench were subducted to the depth greater than 50 km with the oceanic plate (Scholl and von Huene 2007). However, most of the sediments have positive buoyancy relative to the upper mantle and rise to the bottom of the arc crust (Behn et al., 2011; Hacker et al., 2011). As discussed above, the A-type granites were possibly formed by high-temperature (up to 906 °C) and low-pressure setting (<0.5 GPa). At the same time, the coexistence of A-type granites, charnockites, adakites, and sanukitoid dikes in the West Junggar also indicates a high-temperature regime during the Late Carboniferous. Therefore, an additional heat source from the mantle is required to produce the high-temperature rock assemblages in the West Junggar. Asthenospheric upwelling induced by ridge subduction was speculated to have occurred in the West Junggar during the Late Carboniferous (Geng et al., 2009; Tang et al., 2010, 2012; Yin et al., 2010, 2013, 2015). This process can also lead to the melting of the underlying sediments. Subsequently, these sediment melts rose and mixed with the melts in the middle crust to form A-type granites.

The West Junggar arc was developed from Cambrian to Carboniferous (Xiao et al., 2008). In the Early to Late Carboniferous, a large volume of volcanic rocks erupted in the West Junggar (Geng et al., 2011; Choulet et al., 2012). Meanwhile, plutons with 330–311 Ma gabbroic and dioritic compositions were emplaced (Tang et al., 2019). These rocks are characterized by low $\delta^{18}\text{O}$ values (4.5‰–6.9‰), implying their magma sources were dominated either by underplated mantle-derived rocks or by unaltered oceanic crust (Fig. 9B). These post-311 Ma intrusive rocks are mainly granitic in composition and have much higher $\delta^{18}\text{O}$ values (7.2‰ to +11.9‰) (Fig. 9B). The abrupt change in oxygen isotopic compositions may indicate that a significant amount of

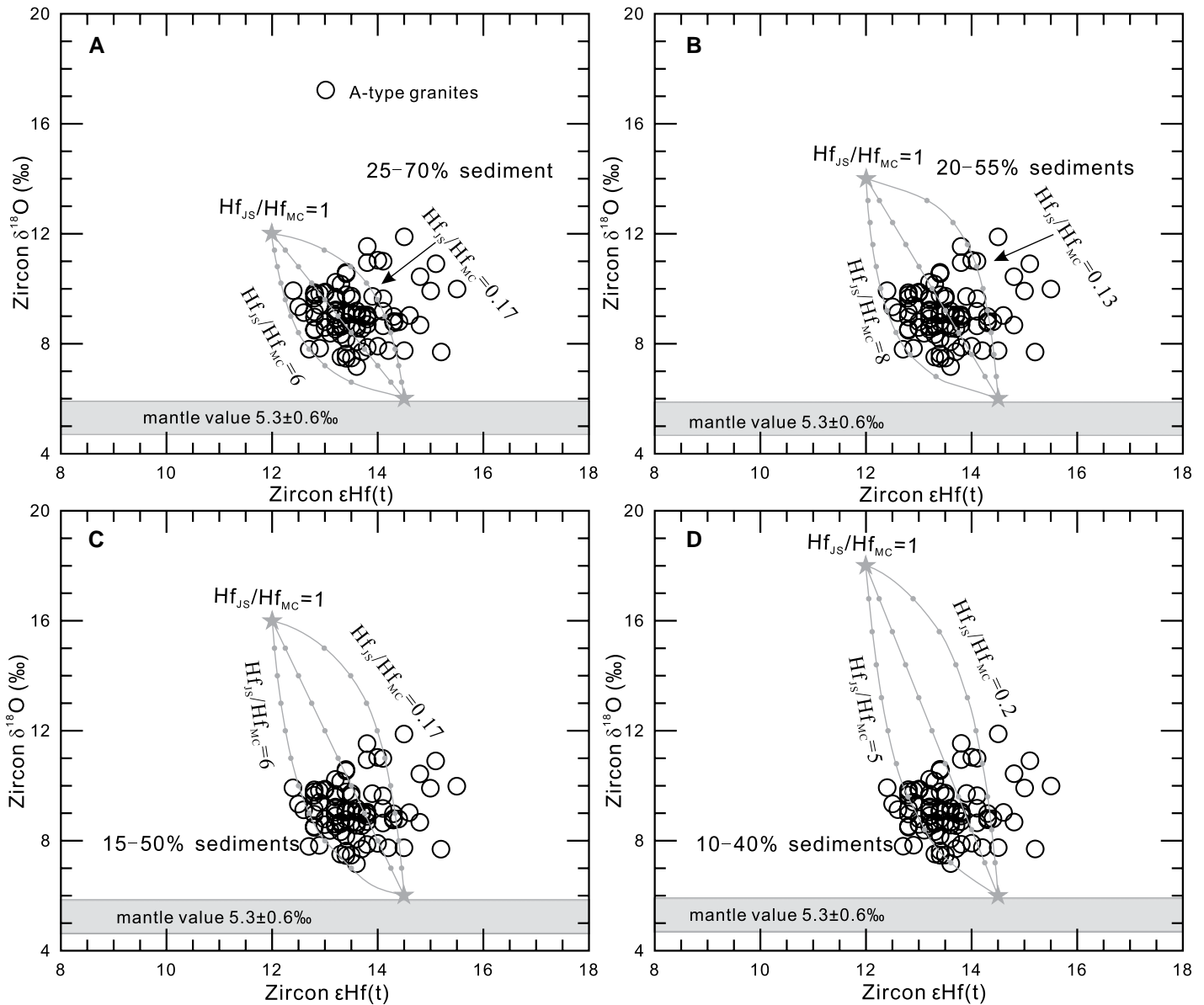


Figure 12. Zircon $\epsilon\text{Hf}(t)$ versus zircon $\delta^{18}\text{O}$ diagrams for magmatic zircon of the Late Carboniferous to Early Permian A-type granites in the West Junggar, NW China. Juvenile sediment (i.e., greywacke) and middle crust are chosen as two plausible endmembers. The Early Carboniferous volcanogenic sedimentary rocks in studied area have positive zircon $\epsilon\text{Hf}(t)$ values of +5 to +17 (85% of the data are between +10 and +16), and the lowest $\epsilon\text{Hf}(t)$ value in the A-type granites is +12. Thus, we assume that $\epsilon\text{Hf}(t)$ value of juvenile weathered sediment is +12. Oxygen isotopic variations in greywackes on Earth are between 10‰ and 19‰ (Bindeman, 2008). We selected four groups of oxygen isotope values from 12‰, 14‰, 16‰, 18‰, respectively, since there is no available oxygen isotope of greywacke in the studied area as a reference. The $\epsilon\text{Hf}(t)$ and $\delta^{18}\text{O}$ values of the Late Carboniferous diorite and granodiorite in the West Junggar are +12 to +17.5 and 5‰ to 6.9‰, respectively (Tang et al., 2019). We assume that $\epsilon\text{Hf}(t)$ and $\delta^{18}\text{O}$ values of middle crust are +14.5 and 6‰, respectively. $\text{Hf}_{\text{JS}}/\text{Hf}_{\text{MC}}$ is the ratio of Hf concentration in the juvenile weathered sediment over parental middle crust indicated for each mixing curves, and the small ticks on the curves represent 10% mixing increments by assuming the juvenile middle crust and the juvenile weathered sediment. The field of mantle-derived zircon (Valley, 2003) is shown for comparison. Four model calculations were carried out and obtain the four proportions of sediment addition, i.e., 25%–70%, 20%–55%, 15%–50%, 10%–40%, respectively. All four results show that sediments play an important role in the formation of A-type granites. Among them, the oxygen isotope value of greywacke is 16‰, the A-type granites contain 15%–50% sediments, close to the model result of rare earth elements (Fig. 11). JS—juvenile sediment; MC—middle crust.

sedimentary materials were deeply buried by subduction in the accretionary prism and were melted post-311 Ma. It is also a manifestation of the transformation of the kinetic process

(i.e., normal subduction to ridge subduction). It was the melting of the juvenile sedimentary material in the oceanic arc system that promoted crustal maturation in the region.

CONCLUSIONS

In situ zircon laser ablation–inductively coupled plasma–mass spectrometry dating revealed

that the A-type granites were emplaced in the period of 307–298 Ma. All these A-type granites have similar Hf isotope compositions (+12.4 to +15.5) indicating a supra-chondritic magma source. However, their high $\delta^{18}\text{O}_{\text{Zrn}}$ (7.2‰–11.9‰) values show that their magma sources contained a large amount of supracrustal materials (~50%). This study shows that zircon Hf-O isotopic components are effective in deciphering the involvement of the juvenile supracrustal material in the source of granitic magma and thus tracing the recycling of juvenile supracrustal materials. The study shows that the re-melting of juvenile sediments in oceanic arc systems may promote crustal maturation.

ACKNOWLEDGMENTS

We thank Professor Brad Singer and Professor Haibo Zou for editorial handling and Kwan-Nang Pang and two anonymous reviewers for constructive reviews and comments that have greatly improved the quality of this paper. This study was supported by the National Key Research and Development Project “Key scientific issues of transformative technology” (grant number 2019YFA0708601), National Key Research and Development 445 Program of China (2017YFC0601206), National Science Foundation of China (grant numbers 41888101, 41873060, and 41830216), the China Geological Survey (grant numbers DD20190001 and DD20190004), the Fund from the Key Laboratory of Deep-Earth Dynamics of Ministry of Natural Resources (J1901-5), the China Geological Survey (grant numbers DD20190001 and DD20190004), and Hong Kong Research Grants Council (grant numbers 17303415 and 17302317). This is a contribution to the International Geoscience Programme 662.

REFERENCES CITED

- Andersen, T., 2002, Correction of common lead in U-Pb analyses that do not report ^{204}Pb : *Chemical Geology*, v. 192, p. 59–79, [https://doi.org/10.1016/S0009-2541\(02\)00195-X](https://doi.org/10.1016/S0009-2541(02)00195-X).
- Altherr, F.F., Holl, A., Hegner, E., Langer, C., and Kreuzer, H., 2000, High potassium, calc-alkaline I-type plutonism in the European Variscides: Northern Vosges (France) and northern Schwarzwald (Germany): *Lithos*, v. 50, p. 51–73.
- Barbarin, B., 1999, A review of the relationships between granitoid types, their origins and their geodynamic environments: *Lithos*, v. 46, p. 605–626, [https://doi.org/10.1016/S0024-4937\(98\)00085-1](https://doi.org/10.1016/S0024-4937(98)00085-1).
- Behn, M.D., Kelemen, P.B., Hirth, G., Hacker, B.R., and Massonne, H., 2011, Diapirs as the source of the sediment signature in arc lavas: *Nature Geoscience*, v. 4, p. 641–646, <https://doi.org/10.1038/ngeo1214>.
- Bindeman, I., 2008, Oxygen isotopes in mantle and crustal magmas as revealed by single crystal analysis: *Minerals: Inclusions and volcanic processes*, v. 69, p. 445–478.
- Bindeman, I.N., Eiler, J.M., Yodanis, G.M., Tatsumi, Y., Stern, C.R., Grove, T.L., Portnyagin, M., Hoernle, K., and Danyushevsky, L.V., 2005, Oxygen isotope evidence for slab melting in modern and ancient subduction zones: *Earth and Planetary Science Letters*, v. 235, p. 480–496, <https://doi.org/10.1016/j.epsl.2005.04.014>.
- Black, L.P., Kamo, S.L., Allen, C.M., Aleinikoff, J.N., Davis, D.W., Korsch, R.J., and Foudoulis, C., 2003, TEMORA 1: A quality zircon standard for Phanerozoic U-Pb geochronology: *Chemical Geology*, v. 200, p. 155–170, [https://doi.org/10.1016/S0009-2541\(03\)00165-7](https://doi.org/10.1016/S0009-2541(03)00165-7).
- Blichert-Toft, J., and Albareda, F., 1997, The Lu-Hf geochemistry of chondrites and the evolution of the mantle-crust system: *Earth and Planetary Science Letters*, v. 148, p. 243–258, [https://doi.org/10.1016/S0012-821X\(97\)00040-X](https://doi.org/10.1016/S0012-821X(97)00040-X).
- Bolhar, R., Weaver, S.D., Whitehouse, M.J., Palin, J.M., Woodhead, J.D., and Cole, J.W., 2008, Sources and evolution of arc magmas inferred from coupled O and Hf isotope systematics of plutonic zircons from the Creteaceous Separation Point Suite (New Zealand): *Earth and Planetary Science Letters*, v. 268, p. 312–324, <https://doi.org/10.1016/j.epsl.2008.01.022>.
- Bonin, B., 2007, A-type granites and related rocks: Evolution of a concept, problems and prospects: *Lithos*, v. 97, p. 1–29, <https://doi.org/10.1016/j.lithos.2006.12.007>.
- Cawood, P.A., Kroner, A., Collins, W.J., Kusky, T.M., Mooney, W.D., and Windley, B.F., 2009, Accretionary orogens through Earth history, in Cawood, P.A., and Kröner, A., eds., *Earth Accretionary Systems in Space and Time*: Geological Society of London, Special Publications, v. 318, p. 1–36, <https://doi.org/10.1144/SP318.1>.
- Chappell, B.W., and White, A.J.R., 1992, I- and S-type granites in the Lachlan Fold Belt: *Earth and Environmental Science Transactions of the Royal Society of Edinburgh*, v. 83, no. 1–2, p. 1–26, <https://doi.org/10.1017/S0263593300007720>.
- Chen, B., and Arakawa, Y., 2005, Elemental and Nd-Sr isotopic geochemistry of granitoids from the West Junggar foldbelt (NW China), with implications for Phanerozoic continental growth: *Geochimica et Cosmochimica Acta*, v. 69, p. 1307–1320, <https://doi.org/10.1016/j.gca.2004.09.019>.
- Chen, B., and Jahn, B.M., 2004, Genesis of post-collisional granitoids and basement nature of the Junggar Terrane, NW China: Nd-Sr isotope and trace element evidence: *Journal of Asian Earth Sciences*, v. 23, p. 691–703, [https://doi.org/10.1016/S1367-9120\(03\)00118-4](https://doi.org/10.1016/S1367-9120(03)00118-4).
- Chen, J.F., Han, B.F., Ji, J.Q., Zhang, L., Xu, Z., He, G.Q., and Wang, T., 2010, Zircon U–Pb ages and tectonic implications of Paleozoic plutons in northern West Junggar, North Xinjiang, China: *Lithos*, v. 115, p. 137–152, <https://doi.org/10.1016/j.lithos.2009.11.014>.
- Choulet, F., Cluzel, D., Faure, M., Lin, W., Wang, B., Chen, Y., Wu, F.Y., and Ji, W.B., 2012, New constraints on the pre-Permian continental crust growth of Central Asia (West Junggar, China) by U–Pb and Hf isotopic data from detrital zircon: *Terra Nova*, v. 24, p. 189–198, <https://doi.org/10.1111/j.1365-3121.2011.01052.x>.
- Collins, W.J., 1996, Lachlan Fold Belt granitoids: Products of three-component mixing: *Transactions of the Royal Society of Edinburgh. Earth Sciences*, v. 87, p. 171–181, <https://doi.org/10.1017/S0263593300006581>.
- Collins, W.J., Beams, S.D., White, A.J.R., and Chappell, B.W., 1982, Nature and origin of A-type granites with particular reference to southeastern Australia: Contributions to Mineralogy and Petrology, v. 80, p. 189–200, <https://doi.org/10.1007/BF00374895>.
- Dhuime, B., Hawkesworth, C., and Cawood, P., 2011, When continents formed: *Science*, v. 331, p. 154–155, <https://doi.org/10.1126/science.1201245>.
- Eby, G.N., 1990, The A-type granitoids a review of their occurrence and chemical characteristics and speculations their petrogenesis: *Lithos*, v. 26, p. 115–134, [https://doi.org/10.1016/0024-4937\(90\)90043-Z](https://doi.org/10.1016/0024-4937(90)90043-Z).
- Eby, G.N., 1992, Chemical subdivision of the A-type granitoids: Petrogenetic and tectonic implications: *Geology*, v. 20, p. 641–644, [https://doi.org/10.1130/0091-7613\(1992\)020<0641:CSOTAT>2.3.CO;2](https://doi.org/10.1130/0091-7613(1992)020<0641:CSOTAT>2.3.CO;2).
- Frost, C.D., and Frost, B.R., 2011, On ferroan (A-type) granitoids: their compositional variability and modes of origin: *Journal of Petrology*, v. 52, p. 39–53, <https://doi.org/10.1093/petrology/egq070>.
- Frost, B.R., Barnes, C.G., Collins, W.J., Arculus, R.J., Ellis, D.J., and Frost, C.D., 2001, A geochemical classification for granitic rocks: *Journal of Petrology*, v. 42, p. 2033–2048, <https://doi.org/10.1093/petrology/42.11.2033>.
- Frost, C., Frost, B., Bell, J., and Chamberlain, K., 2002, The relationship between A-type granites and residual magmas from anorthositic: Evidence from the northern Sherman batholith, Laramie Mountains, Wyoming, USA: *Precambrian Research*, v. 119, p. 45–71, [https://doi.org/10.1016/S0301-9268\(02\)00117-1](https://doi.org/10.1016/S0301-9268(02)00117-1).
- Geng, H.Y., Sun, M., Yuan, C., Xiao, W.J., Zhao, G.C., Zhang, L.F., Wong, K., and Wu, F.Y., 2009, Geochemical, Sr–Nd and zircon U–Pb–Hf isotopic studies of Late Carboniferous magmatism in the West Junggar, Xinjiang: Implications for ridge subduction?: *Chemical Geology*, v. 266, p. 364–389, <https://doi.org/10.1016/j.chemgeo.2009.07.001>.
- Geng, H.Y., Sun, M., Yuan, C., Zhao, G.C., and Xiao, W.J., 2011, Geochemical and geochronological study of early Carboniferous volcanic rocks from the West Junggar: Petrogenesis and tectonic implications: *Journal of Asian Earth Sciences*, v. 42, p. 854–866, <https://doi.org/10.1016/j.jseas.2011.01.006>.
- Gill, T.B., 1981, *Orogenic Andesite and Plate Tectonics*: Berlin, Germany, Springer-Verlag, 390 p., <https://doi.org/10.1007/978-3-642-68012-0>.
- Griffin, W.L., Pearson, N.J., Belousova, E.A., Jackson, S.R., van Achterbergh, E., O’Reilly, S.Y., and Shee, S.R., 2000, The Hf isotope composition of cratonic mantle: LAM-MC-ICPMS analysis of zircon megacrysts in kimberlites: *Geochimica et Cosmochimica Acta*, v. 64, p. 133–147, [https://doi.org/10.1016/S0016-7037\(99\)00343-9](https://doi.org/10.1016/S0016-7037(99)00343-9).
- Hacker, B.R., Kelemen, P.B., and Behn, M.D., 2011, Differentiation of the continental crust by reamination: *Earth and Planetary Science Letters*, v. 307, p. 501–516, <https://doi.org/10.1016/j.epsl.2011.05.024>.
- Han, B.F., Wang, S.G., Jahn, B.M., Hong, D.W., Kagami, H., and Sun, Y.L., 1997, Depleted-mantle source for the Ulungur River A-type granites from North Xinjiang, China: Geochemistry and Nd–Sr isotopic evidence, and implications for Phanerozoic crustal growth: *Chemical Geology*, v. 138, p. 135–159, [https://doi.org/10.1016/S0009-2541\(97\)00003-X](https://doi.org/10.1016/S0009-2541(97)00003-X).
- Han, Y.G., and Zhao, G.C., 2018, Final amalgamation of the Tianshan and Junggar orogenic collage in the southwestern Central Asian Orogenic Belt: Constraints on the closure of the Paleo-Asian Ocean: *Earth-Science Reviews*, v. 186, p. 129–152, <https://doi.org/10.1016/j.earscirev.2017.09.012>.
- Han, Y.G., Zhao, G.C., Sun, M., Eizenhöfer, P.R., Hou, W.Z., Zhang, X.R., Liu, D.X., Wang, B., and Zhang, G.W., 2015, Paleozoic accretionary orogenesis in the Paleo-Asian Ocean: Insights from detrital zircons from Silurian to Carboniferous strata at the northwestern margin of the Tarim Craton: *Tectonics*, v. 34, p. 334–351, <https://doi.org/10.1002/2014TC003668>.
- Harrison, T.M., Blichert-Toft, J., Müller, W., Albareda, F., Holden, P., and Mojzsis, S.J., 2005, Heterogeneous Hadean hafnium: Evidence of continental crust at 4.4 to 4.5 Ga: *Science*, v. 310, p. 1947–1950, <https://doi.org/10.1126/science.1117926>.
- Healy, B., Collins, W.J., and Richards, S.W., 2004, A hybrid origin for Lachlan S-type granites: the Murrumbidgee Batholith example: *Lithos*, v. 78, p. 197–216, <https://doi.org/10.1016/j.lithos.2004.04.047>.
- Hopkinson, T.N., Harris, N.B.W., Warren, C.J., Spencer, C.J., Roberts, N.M.W., Horstwood, M.S.A., Parrish, R.R., and EIMF, 2017, The identification and significance of pure sediment-derived granites: *Earth and Planetary Science Letters*, v. 467, p. 57–63, <https://doi.org/10.1016/j.epsl.2017.03.018>.
- Huang, H.Q., Li, X.H., Li, W.X., and Li, Z.X., 2011, Formation of high $\delta^{18}\text{O}$ fayalite-bearing A-type granite by high temperature melting of granulitic metasedimentary rocks, southern China: *Geology*, v. 39, p. 903–906, <https://doi.org/10.1130/G32080.1>.
- Jackson, S.E., Pearson, N.J., Griffin, W.L., and Belousova, E.A., 2004, The application of laser ablation-inductively coupled plasma-mass spectrometry to in situ U–Pb zircon geochronology: *Chemical Geology*, v. 211, p. 47–69, <https://doi.org/10.1016/j.chemgeo.2004.06.017>.
- Jahn, B.M., Wu, F.Y., and Chen, B., 2000, Massive granitoid generation in central Asia: Nd isotopic evidence and implication for continental growth in the Phanerozoic: *Episodes*, v. 23, p. 82–92, <https://doi.org/10.18814/epiiugs2000/v23i2/001>.
- Jeon, H., Williams, I.S., and Chappell, B.W., 2012, Magma to mud to magma: Rapid crustal recycling by Permian granite magmatism near the eastern Gondwana margin: *Earth and Planetary Science Letters*, v. 319–320, p. 104–117, <https://doi.org/10.1016/j.epsl.2011.12.010>.

- Johnson, M.C., and Plank, T., 1999, Dehydration and melting experiments constrain the fate of subducted sediments: *Geochemistry, Geophysics, Geosystems*, v. 1, no. 12, <https://doi.org/10.1029/1999GC000014>.
- Kemp, A.L., Hawkesworth, C.J., Paterson, B.A., and Kinny, P.D., 2006, Episodic growth of the Gondwana supercontinent from hafnium and oxygen isotopes in zircon: *Nature*, v. 439, p. 580–583, <https://doi.org/10.1038/nature04505>.
- Kemp, A.L.S., Hawkesworth, C.J., Foster, G.L., Paterson, B.A., Woodhead, J.D., Hergt, J.M., Gray, C.M., and Whitehouse, M.J., 2007, Magmatic and crustal differentiation history of granitic rocks from Hf-O isotopes in zircon: *Science*, v. 315, p. 980–983, <https://doi.org/10.1126/science.1136154>.
- Kita, N.T., Ushikubo, T., Fu, B., and Valley, J.W., 2009, High precision SIMS oxygen isotope analysis and the effect of sample topography: *Chemical Geology*, v. 264, p. 43–57, <https://doi.org/10.1016/j.chemgeo.2009.02.012>.
- Lackey, J.S., Valley, J.W., and Saleeby, J.B., 2005, Supracrustal input to magmas in the deep crust of Sierra Nevada batholith: Evidence from high- $\delta^{18}\text{O}$ zircon: *Earth and Planetary Science Letters*, v. 235, p. 315–330, <https://doi.org/10.1016/j.epsl.2005.04.003>.
- Li, X.H., Long, W.G., Li, Q.L., Liu, Y., Zheng, Y.F., Yang, Y.H., Chamberlain, K.R., Wan, D.F., Guo, C.H., Wang, X.C., and Tao, H., 2010b, Penglai zircon megacrysts: A potential new working reference material for microbeam determination of Hf-O isotopes and U-Pb age: *Geostandards and Geoanalytical Research*, v. 34, p. 117–134, <https://doi.org/10.1111/j.1751-908X.2010.00036.x>.
- Li, X.H., Tang, G.Q., Gong, B., Yang, Y.H., Hou, K.J., Hu, Z.C., Li, Q.L., Liu, Y., and Li, W.X., 2013, Qinghu zircon: A working reference for microbeam analysis of U-Pb age and Hf and O isotopes: *Chinese Science Bulletin*, v. 58, p. 4647–4654, <https://doi.org/10.1007/s11434-013-5932-x>.
- Liu, B., Han, B.F., Chen, J.F., Ren, R., Zheng, B., Wang, Z.Z., and Feng, L.X., 2017, Closure time of the Junggar-Balkhash Ocean: Constraints from Late Paleozoic volcano-sedimentary sequences in the Barleik Mountains, West Junggar, NW China: *Tectonics*, v. 36, p. 2823–2845, <https://doi.org/10.1002/2017TC004606>.
- Liu, Y.S., Gao, S., Hu, Z.C., Gao, C.G., Zong, K.Q., and Wang, D.B., 2010, Continental and oceanic crust recycling-induced melt-petrogenesis interactions in the Trans-North China Orogen: U-Pb dating, Hf isotopes and trace elements in zircons from mantle xenoliths: *Journal of Petrology*, v. 51, p. 537–571, <https://doi.org/10.1093/petrology/egg082>.
- Loiselle, M., and Wones, D., 1979, Characteristics and origin of anorogenic granites: *Geological Society of America Abstracts with Programs*, v. 11, p. 468.
- Ludwig, K.R., 2003, Mathematical-statistical treatment of data and errors for $^{230}\text{Th}/\text{U}$ geochronology: *Uranium-Series Geochemistry: Reviews in Mineralogy and Geochemistry*, v. 52, p. 631–656, <https://doi.org/10.2113/0520631>.
- Maniar, P.D., and Piccoli, P.M., 1989, Tectonic discrimination of granites: *Geological Society of America Bulletin*, v. 101, p. 635–643, [https://doi.org/10.1130/0016-7606\(1989\)101<0635:TDOG>2.3.CO;2](https://doi.org/10.1130/0016-7606(1989)101<0635:TDOG>2.3.CO;2).
- McCulloch, M.T., Gregory, R.T., Wasserburg, G.J., and Taylor, H.P., 1980, A neodymium, strontium, and oxygen isotope study of the Cretaceous Samail Ophiolite and implications for the petrogenesis and seawater-hydrothermal alteration of oceanic crust: *Earth and Planetary Science Letters*, v. 46, p. 201–211, [https://doi.org/10.1016/0012-821X\(80\)90006-0](https://doi.org/10.1016/0012-821X(80)90006-0).
- McKenzie, D., and O’Nions, R.K., 1991, Partial melt distributions from inversion of rare earth element concentrations: *Journal of Petrology*, v. 32, p. 1021–1091, <https://doi.org/10.1093/petrology/32.5.1021>.
- Middlemost, E.A.K., 1994, Naming materials in the magma igneous rock system: *Earth-Science Reviews*, v. 37, p. 215–224, [https://doi.org/10.1016/0012-8252\(94\)90029-9](https://doi.org/10.1016/0012-8252(94)90029-9).
- Morel, M.L.A., Nebel, O., and Nebel-Jacobsen, Y.J., 2008, Hafnium isotope characterization of the GJ-1 zircon reference material by solution and laser ablation MC-ICPMS: *Chemical Geology*, v. 255, p. 231–235, <https://doi.org/10.1016/j.chemgeo.2008.06.040>.
- Rapp, R., Shimizu, N., and Norman, M., 2003, Growth of early continental crust by partial melting of eclogite: *Nature*, v. 425, p. 605–609, <https://doi.org/10.1038/nature02031>.
- Rudnick, R.L., and Gao, S., 2014, Composition of the continental crust, in H.D. Holland, and K.K. Turekian, eds., *Treatise on Geochemistry (Second Edition)*: Oxford, UK, Elsevier, p. 1–51, <https://doi.org/10.1016/B978-0-08-095975-7.00301-6>.
- Scholl, D.W., and von Huene, R., 2007, Crustal recycling at modern subduction zones applied to the past—issues of growth and preservation of continental basement, mantle geochemistry, and supercontinent reconstruction, in Hatcher, R.D., Carlson, M.P., McBride, J.H., and Catalán, J.R.M., eds., *4D Framework of Continental Crust*: Geological Society of America Memoir, v. 200, p. 9–32, [https://doi.org/10.1130/2007.1200\(02\)](https://doi.org/10.1130/2007.1200(02)).
- Sláma, J., Košler, J., Condon, D.J., Crowley, J.L., Gerdes, A., Hanchar, J.M., Horstwood, M.S.A., Morris, G.A., Nasdala, L., Norberg, N., Schaltegger, U., Schoene, B., Tubrett, M.N., and Whitehouse, M.J., 2008, Plešovice zircon: A new natural reference material for U-Pb and Hf isotopic microanalysis: *Chemical Geology*, v. 249, p. 1–35, <https://doi.org/10.1016/j.chemgeo.2007.11.005>.
- Spencer, C.J., Kirkland, C.L., and Taylor, R.J.M., 2016, Strategies towards statistically robust interpretations of in situ U-Pb zircon geochronology: *Geoscience Frontiers*, v. 7, p. 581–589, <https://doi.org/10.1016/j.gsf.2015.11.006>.
- Sun, S.S., and McDonough, W.F., 1989, Chemical and isotopic systematics of oceanic basalt: Implications for mantle compositions and processes, in Saunders, A.D., and Norry, M.J., eds., *Magmatism in the Ocean Basins*: Geological Society of London, Special Publications, v. 42, p. 313–345, <https://doi.org/10.1144/GSL.SP.1989.042.01.19>.
- Tang, G.J., Wang, Q., Wyman, D.A., Li, Z.X., Zhao, Z.H., Jia, X.H., and Jiang, Z.Q., 2010, Ridge subduction and crustal growth in the Central Asian Orogenic Belt: Evidence from Late Carboniferous adakites and high-Mg diorites in the western Junggar region, northern Xinjiang (west China): *Chemical Geology*, v. 277, p. 281–300, <https://doi.org/10.1016/j.chemgeo.2010.08.012>.
- Tang, G.J., Wang, Q., Wyman, D.A., Li, Z., Xu, Y.G., and Zhao, Z.H., 2012, Recycling oceanic crust for continental crustal growth: Sr-Nd-Hf isotopic evidence from granitoids in the western Junggar region, NW China: *Lithos*, v. 128, p. 73–83, <https://doi.org/10.1016/j.lithos.2011.11.003>.
- Tang, G.J., Wang, Q., Wyman, D.K., and Dan, W., 2019, Crustal maturation through chemical weathering and crustal recycling revealed by Hf-O-B isotopes: *Earth and Planetary Science Letters*, v. 524, no. 115709, <https://doi.org/10.1016/j.epsl.2019.115709>.
- Tani, K., Fiske, R.S., Dunkley, D.J., Ishizuka, O., Oikawa, T., Isobe, I., and Tatsumi, Y., 2011, The Izu Peninsula, Japan: Zircon geochronology reveals a record of intra-oceanic rear-arc magmatism in an accreted block of Izu-Bonin upper crust: *Earth and Planetary Science Letters*, v. 303, p. 225–239, <https://doi.org/10.1016/j.epsl.2010.12.052>.
- Tao, H.F., Sun, S., Wang, Q.C., Yang, X.F., and Jiang, L., 2014, Petrography and geochemistry of lower carboniferous greywacke and mudstones in Northeast Junggar, China: Implications for provenance, source weathering, and tectonic setting: *Journal of Asian Earth Sciences*, v. 87, p. 11–25, <https://doi.org/10.1016/j.jseaes.2014.02.007>.
- Tatsumi, Y., Shukuno, H., Tani, K., Takahashi, N., Kodaira, S., and Kogiso, T., 2008, Structure and growth of the Izu-Bonin-Mariana arc crust: 2. Role of crust-mantle transformation and the transparent Moho in arc crust evolution: *Journal of Geophysical Research*, *Solid Earth*, v. 113, <https://doi.org/10.1029/2007JB005121>.
- Valley, J.W., 2003, Oxygen isotopes in zircon: Reviews in Mineralogy and Geochemistry, v. 53, p. 343–385, <https://doi.org/10.2113/0530343>.
- Valley, J.W., Chiarenzelli, J.R., and McLelland, J.M., 1994, Oxygen isotope geochemistry of zircon: *Earth and Planetary Science Letters*, v. 126, p. 187–206, [https://doi.org/10.1016/0012-821X\(94\)90106-6](https://doi.org/10.1016/0012-821X(94)90106-6).
- Valley, J.W., Lackey, J.S., Cavosie, A.J., Clechenko, C.C., Spicuzza, M.J., Basei, M.A.S., Bindeman, I.N., Ferreira, V.P., Sial, A.N., King, E.M., Peck, W.H., Sinha, A.K., and Wei, C.S., 2005, 4.4 billion years of crustal maturation: oxygen isotope ratios of magmatic zircon: *Contributions to Mineralogy and Petrology*, v. 150, p. 561–580, <https://doi.org/10.1007/s00410-005-0025-8>.
- Wang, Q., Hawkesworth, C.J., Wyman, D., Chung, S.L., Wu, F.Y., Li, X.H., Li, Z.X., Guo, G.N., Zhang, X.Z., Tang, G.J., Dan, W., Ma, L., and Dong, Y.H., 2016, Pliocene-Quaternary crustal melting in central and northern Tibet and insights into crustal flow: *Nature Communications*, v. 7, no. 11888, <https://doi.org/10.1038/ncomms11888>.
- Whalen, J.B., Currie, K.L., and Chappell, B.W., 1987, A-type granites: Geochemical characteristics, discrimination and petrogenesis: *Contributions to Mineralogy and Petrology*, v. 95, p. 407–419, <https://doi.org/10.1007/BF00402202>.
- White, A.J.R., and Chappell, B.W., 1977, Ultrametamorphism and granitoid genesis: *Tectonophysics*, v. 43, p. 7–22, [https://doi.org/10.1016/0040-1951\(77\)90003-8](https://doi.org/10.1016/0040-1951(77)90003-8).
- Xia, X.P., Sun, M., Zhao, G.C., Li, H.M., and Zhou, M.F., 2004, Spot zircon U-Pb isotope analysis by ICP-MS coupled with a frequency quintupled (213 nm) Nd-YAG laser system: *Geochemical Journal*, v. 38, p. 191–200, <https://doi.org/10.2343/geochemj.38.191>.
- Xiao, W.J., Han, C.M., Yuan, C., Sun, M., Lin, S.F., Chen, H.L., Li, Z.L., Li, J.L., and Sun, S., 2008, Middle Cambrian to Permian subduction-related accretionary orogenesis of Northern Xinjiang, NW China: Implications for the tectonic evolution of central Asia: *Journal of Asian Earth Sciences*, v. 32, p. 102–117, <https://doi.org/10.1016/j.jseaes.2007.10.008>.
- Yang, Q., Xia, X.P., Zhang, W.F., Zhang, Y.Q., Xiong, B.Q., Xu, Y.G., Wang, Q., and Wei, G.J., 2018, An evaluation of precision and accuracy of SIMS oxygen isotope analysis: *Solid Earth Sciences*, v. 3, p. 81–86, <https://doi.org/10.1016/j.sesci.2018.05.001>.
- Yang, W.-B., Niu, H.-C., Hollings, P., Zurevinski, S.E., and Li, N.-B., 2017, The role of recycled oceanic crust in the generation of alkaline A-type granites: *Journal of Geophysical Research*, *Solid Earth*, v. 122, p. 9775–9783, <https://doi.org/10.1002/2017JB014921>.
- Yin, J.Y., Yuan, C., Sun, M., Long, X.P., Zhao, G.C., Wong, K.P., Geng, H.Y., and Cai, K.D., 2010, Late Carboniferous high-Mg dioritic dikes in Western Junggar, NW China: Geochemical features, petrogenesis and tectonic implications: *Gondwana Research*, v. 17, p. 145–152, <https://doi.org/10.1016/j.gr.2009.05.011>.
- Yin, J.Y., Long, X.P., Yuan, C., Sun, M., Zhao, G.C., and Geng, H.Y., 2013, A Late Carboniferous slab window: Geochronological and geochemical evidence from mafic to intermediate dykes in West Junggar, NW China: *Lithos*, v. 175–176, p. 146–162, <https://doi.org/10.1016/j.lithos.2013.04.005>.
- Yin, J.Y., Chen, W., Xiao, W.J., Yuan, C., Sun, M., Tang, G.J., Yu, S., Long, X.P., Cai, K.D., Geng, H.Y., Zhang, Y., and Liu, X.Y., 2015, Petrogenesis of Early-Permian sanukitoids from West Junggar, Northwest China: implications for Late Paleozoic crustal growth in Central Asia: *Tectonophysics*, v. 662, p. 385–397, <https://doi.org/10.1016/j.tecto.2015.01.005>.
- Yin, J.Y., Chen, W., Xiao, W.J., Yuan, C., Windley, B.F., Yu, S., and Cai, K.D., 2017, Late Silurian-early Devonian adakitic granodiorite, A-type and I-type granites in NW Junggar, NW China: Partial melting of mafic lower crust and implications for slab roll-back: *Gondwana Research*, v. 43, p. 55–73, <https://doi.org/10.1016/j.gr.2015.06.016>.
- Zeng, L.S., Gao, L.E., Xie, K.J., and Zeng, J.L., 2011, Mid-Eocene high Sr/Y granites in the Northern Himalayan Gneiss Domes: Melting thickened northern continental crust: *Earth and Planetary Science Letters*, v. 303, p. 251–266, <https://doi.org/10.1016/j.epsl.2011.01.005>.

SCIENCE EDITOR: BRAD S. HINGOR
ASSOCIATE EDITOR: SAIIBO ZOU

MANUSCRIPT RECEIVED 15 JUNE 2020
REVISED MANUSCRIPT RECEIVED 10 JULY 2020
MANUSCRIPT ACCEPTED 31 OCTOBER 2020

Printed in the USA